Physics – Uspekhi **67** (7) 668 – 693 (2024)

REVIEWS OF TOPICAL PROBLEMS

PACS numbers: **03.67. – a**, **06.20. – f**, **42.50. – p**, 42.50.Dv

Quantum optical metrology

A P Alodjants, D V Tsarev, D A Kuts, S A Podoshvedov, S P Kulik

DOI: https://doi.org/10.3367/UFNe.2024.01.039634

Contents

Abstract. **We review recent progress in the field of optical quantum metrology, with a focus on the analysis of the current level of theoretical and experimental research on the generation, transformation, and measurement of nonclassical states of light, such as $N00N$, squeezed, and hybrid states, which combine transformations of both discrete and continuous variables of a quantized light field. We show how such states can be used to improve the measurement accuracy and to estimate unknown phase parameters in both linear and nonlinear metrology. Significant attention is paid to the description of actual quantum metrology schemes that take the loss of particles, the limited fidelity of photon detectors, and other factors into account. We therefore identify both the ultimate (fundamental) bounds imposed by quantum mechanical uncertainties of the quantities being measured and the bounds due to the effect of classical noise on the propagation and measurements of a quantized field. Of special importance are quantum metrology options based on spontaneous parametric light scattering, which, for more than 50 years, has been an indispensable tool for key accomplishments in quantum optics and related areas of photonics: quantum cryptography, quantum computing, and quantum sensing. In this regard, we analyze the current status of the use of the well-known Hong–Ou–Mandel photon anticorrelation effect and biphoton interference in various quantum metrology approaches in measuring temperature, length, material concentration, and so on. We also discuss the use of biphotons in photometry, radiometry, and sensing for the absolute calibration of modern photon-count detectors, as well as for measurements of the brightness temperature of hot radiation sources. The quantum metrology phenomena, methods, and approaches discussed here in light of the most recent progress on sources and detectors of quantum radiation will be an important tool in developing and practically implementing new schemes and algorithms for quantum processing and information transmission.**

Keywords: quantum measurement, quantum interferometry, spontaneous parametric light scattering, quantum sensing, photometry, radiometry, nonclassical states of light, biphotons, quantum information and computing

A P Alodjants [1, 2, a], **D V Tsarev** [1, 2, b], **D A Kuts** [2, c], **S A Podoshvedov** [2, d], **S P Kulik** [2, 3, e]

[1] ITMO University, Kronverksky prosp. 49A, 197101 St. Petersburg, Russian Federation

[2] South Ural State University, prosp. Lenina 76, 454080 Chelyabinsk, Russian Federation

[3] Lomonosov Moscow State University, Quantum Technology Center, Leninskie gory 1, str. 35, 119991 Moscow, Russian Federation

E-mail: [a] alexander_ap@list.ru, [b] dmitriy_93@mail.ru, [c] tpmchel@yandex.ru, [d] podoshvedovsa@susu.ru, [e] sergei.kulik@physics.msu.ru

Received 28 September 2023, revised 25 December 2023

Uspekhi Fizicheskikh Nauk **194** (7) 711 – 739 (2024)

Translated by S Alekseev

1. Introduction

Increasing the accuracy of primary measuring technologies (sensors and transducers) and their calibration are becoming

progressively more important for modern industry and advanced technologies in developed countries, as is stated in the relevant road maps (see, e.g., [1, 2]) and other national development programs [3]. These relevant technologies include precision instrumentation, positioning and navigation technologies (GPS, GLONASS), mobile communications, and telecommunications to be used in industry, science, medicine, and other areas of human activity. Classical optical measurements are traditionally of major significance here as regards measuring small displacements (of the order of or less than a nanometer) and monitoring and calibrating devices and instruments for modern technological processes [4]. Such measurements are underlain by the universal principles of interferometry, which have long been known from classical optics [5] and are actively being developed for quantum states of light [6, 7].

As a science of measurement, metrology offers two approaches to describing the results of an experiment: using the concepts of the true value and error (deviation from the true value) or using the concepts of the estimate and uncertainty (the measure of doubt in the estimate).[1] The measurement uncertainty, according to these standards, is a parameter pertaining to the measurement result and characterizing the spread of values that could reasonably be assigned to the measured quantity.

From a practical standpoint, the accuracy of classical measurements of physical parameters is determined by noise caused by various defects in technical measuring tools, which, in theory, can be eliminated. As a result, the task of classical metrology has traditionally been to improve the measurement accuracy by developing new methods and approaches to eliminate such imperfections.

With demands on the capabilities of modern technologies increasing worldwide, the requirements for accuracy and uniformity of approaches to measuring various physical quantities are also becoming more stringent, giving rise to one of the tasks of metrology as a science in general [8]. It is obvious in this regard that classical methods and approaches become inapplicable to measurements carried out at the level of quantum limits, which have a fundamental nature [9] and are referred to in the literature as the standard quantum limit (SQL) of the relevant measurements [6]. We note that the concept of SQL was initially formulated by Braginsky [10] in connection with the problem of testing the equivalence principle by estimating the ultimate sensitivity of a quantum mechanical macroscopic oscillator under the action of physically weak forces. Later, this concept was generalized to quantized electromagnetic radiation in a coherent state, whose fluctuations determine the so-called shot noise level in a balanced homodyning scheme [11]. This is justified from a physical standpoint, because the quadratures of a quantized field are analogous to the momentum and coordinates of a quantum mechanical oscillator [12]. However, if the physical measurement scheme, along with the quantized radiation field, also involves a 'true' quantum mechanical oscillator (e.g., a thin membrane in optomechanic experiments), the SQL measurements with this oscillator must be distinguished from those with quantized radiation (cf. [13]).

[1] The approach associated with estimates and uncertainties is used by the international organization for standardization (ISO/IEC Guide 98.3:2008), and, in Russia, the corresponding GOST 34100.3-2017, which provides guidance on the expression of measurement uncertainty, was introduced as a national standard on September 1, 2018.

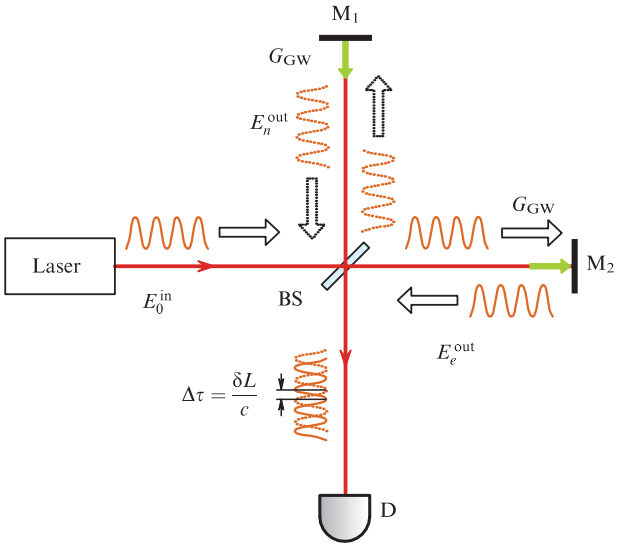

Figure 1. Schematic representation of Michelson interferometer for detecting gravitational waves (GWs), whose action, designated as G_{GW}, reduces to the appearance of small physical displacements, which are reflected in path difference δL for waves in the interferometer arms (4 km in length) [17]. E_0^{in} is field produced by a laser source, $E_{e,n}^{out}$ are fields reflected from mirrors $M_{1,2}$, D is a detector, BS is a semitransparent beamsplitter, and green arrows show small physical displacements due to the action of GWs.

Quantum metrology deals with noise associated with various kinds of uncertainty relations that impose restrictions on the accuracy of quantum measurements (cf. [12]). Over the past 20 years, nonclassical states of light have become an indispensable tool in optical quantum metrology, which allows controlling fluctuations of canonically conjugate quantities — the Hermitian quadrature components that are continuous observable parameters of the electromagnetic field [14].

Importantly, the measurement paradigm in quantum theory, touching upon its foundations, has traditionally been the subject of heated debate (not only in physics) and serves as a source of various paradoxes in quantum mechanics and beyond [15]. The role of the 'measuring device,' which essentially represents a certain physical process in quantum measurement, is enormously greater than that assigned to a device in the classical case [16]. Thus, the task of quantum metrology is not only to eliminate (or minimize) classical noise caused by the technological and design features of measuring devices and setups but also to increase the absolute accuracy of measurements based on controlling the uncertainty ratios of the conjugate physical quantities involved in the measurement process.

The most striking recent example is given by the observation and registration of gravitational waves, which would have been impossible without measuring physically small displacements (of the order of or less than $\delta L \simeq 10^{-18}$ m) with a technologically unique Michelson interferometer (MI) [18] (Fig. 1). These experiments are based on methods and approaches for measuring weak forces in nature, first proposed and studied by Braginsky's group [19] and then developed in various laboratories around the world [17, 20, 21].

A special role in such measurements is played by the coherent squeezed vacuum (CSV) state, which was proposed in [6] and has been successfully used in gravitational wave

detectors for more than 10 years [14]. CSV states are classified among the continuous observables that can contain a macroscopically large number of photons due to the coherent component of the field , which allows them to be used in unique experiments, e.g., in [22]. We also note study [23], where the peculiarities of squeezed states of light used to increase the sensitivity of gravitational antennas were analyzed from the standpoint of the progress achieved in experiments on gravitational wave detection.

It is worth noting that optical methods and approaches in quantum metrology are currently successfully being applied to develop quantum frequency standards [24], quantum magnetic field sensors (magnetometers) [25], and quantum imaging [26], as well as in many other areas that are traditionally associated with quantum technologies (see, e.g., [27]). These methods and approaches developed in optics turned out to be so universal from a practical standpoint that they were laid into the foundation of various metrological applications involving atoms and other material objects that demonstrate a wave nature under appropriate physical conditions (see, e.g., [28–30]).

Quantum magnetic field sensors have an energy resolution per passband of the order of or less than the Planck constant $\hbar$, which quantitatively characterizes the spatial, temporal, and field resolution of a magnetic field sensor. In practical terms, the purposes of such devices are diverse: for example, they can account for the minimum possible change in the electromagnetic field allowed by a sensor and determined by the signal-to-noise ratio, the bandwidth, the measurement duration, the size of the sensor area, its operating temperature, and so on (see, e.g., [25]). Methods for generating and measuring single-photon light in the visible and near-infrared (IR) ranges play a major role in modern quantum sensing. We refer the reader to review [31], whose relevance is preserved to this day and which combines an in-depth analysis of experimental methods with methodological and interpretational aspects of the study of quantum optical effects associated with quantization and statistical properties of the field and the peculiarities of detection in different regimes and the use in quantum metrology.

The majority of devices under development in atomic optics — optical clocks, gravimeters, and magnetometers — are based on ultracold atomic ensembles placed in optical lattices and controlled by electromagnetic pulses (cf. [32]). The accuracy in determining frequency has been achieved at the level of 2.5×10^{-19} or 100 μHz at an optical frequency [33]. Going beyond the SQL is possible if quantum atomic fluctuations are controlled using nonclassical states of light; for this, one can use both optical squeezed states of light, which are discussed in what follows, and atomically squeezed states involving spin squeezing, which, in addition, allow achieving atomic entanglement [34, 35]. Due to measurements carried out beyond the SQL level, these devices demonstrate a high stability in frequency, but with fewer atoms. Among such systems, we single out atomic clocks [36] and magnetic field sensors [37]. In particular, cells containing a macroscopic number of atoms $N \simeq 10^{12}$ allow attaining a sensitivity of magnetic field measurements of less than 1 fT $\text{Hz}^{-1/2}$ [38], which is comparable to magnetometers containing a much greater number of atoms [39].

Recently, technologies have been under development worldwide for manufacturing atomic chips containing Bose–Einstein condensates (BECs) of atoms, to be used in quantum metrology and sensors involving the effects of gravity [40, 41]. Precisely such systems are promising for gravimeters to be placed in orbit [28]. The advantages of atomic chips are their compactness and the ability to create sufficiently deep magnetic traps. The main challenges in operating such systems are associated with the need to maintain low temperatures (tens of μK and below) to ensure the overall physical coherence of the atomic system. Of course, the study of such systems is of great interest for the development of quantum metrology in Russia but requires separate consideration and analysis, because their practical use is associated with considerable capital investments to create the necessary infrastructure, to master the technology for its use, and so on [28]. In addition, optical metrology is an integral part of quantum sensing [42, 43], which is a subtechnology of the high-tech field of quantum technologies, which has been actively developed in recent years throughout the world.

This review is devoted to topical problems in quantum metrology based on the use of optical systems that already today can provide a high measurement accuracy at the SQL level or even overcoming it in modern problems of photonics, laser technology, and processing and transmitting quantum information.

Overcoming the SQL in measuring small phase shifts was predicted theoretically and demonstrated experimentally for various optical systems containing two effectively coupled (interfering) modes and using nonclassical squeezed or entangled quantum states as the initial states for Mach–Zehnder interferometers (MZIs) [6, 7, 44], gyroscopes (Sagnac interferometers) [45], lithographs [46, 47], radars [48], and lidars [49, 50]. Special attention is devoted to issues of the implementation of so-called 'quantum illumination' devices [51], which, although outside the scope of quantum sensing/metrology, are based on methods of generating and detecting nonclassical light and are actively discussed in view of their potential applications.

In particular, as shown in [52–54], with a small average number of photons, CSV states can overcome the SQL and saturate the so-called Heisenberg limit (HL) in measurements of an unknown phase parameter with an MZI. At the same time, it is already intuitively clear that the corpuscular properties of light must already be taken into account to a certain extent by the quantum metrology problem setup in and of itself. In this regard, the minimal resource for such measurements is individual photons, often considered in the literature as discrete-variable systems of a quantized light field. Because high-precision quantum measurement schemes (including those used in modern optical quantum information technologies) are underlain by quantum N-photon interference (see, e.g., [55]), an extremely important task of quantum metrology is to prepare correlated states of two or more photons. This was noted by Klyshko [56], who proposed to use the link between spontaneous and stimulated two-photon transitions to determine the spectral brightness and effective temperature of incoherent light. This measurement technique was subsequently verified experimentally [57], and today it deservedly occupies its rightful place in photometry and in problems of calibrating light detectors [31, 58], offering an example of a simple and accessible method for assessing the spectral distributions of quantum efficiency. Unfortunately, although absolute quantum photometry was proposed and tested quite a long time ago, it has not yet attained the metrological level. This is primarily due to the difficulties in dealing with the nonidealities of the proposed optical

setups: losses, matching and filling of modes, and so on. Obviously, this technique can be improved based on current advancements in quantum optics and in view of pressing practical problems associated with measuring the temperatures of hot (significantly above room temperature) radiation sources in a wide range.

In what follows, we present an analysis of modern trends in the field of optical quantum measurements and their practical capabilities in solving quantum metrology problems. We note that these areas are closely related to other (nonoptical) methods of high-precision measurements and sensing in atomic physics, superconducting systems, and micro- and nanostructures, which have been the subject of a large number of recent studies (see, e.g., [59]). But it is the paradigm of optical quantum measurements associated with manifestations of coherence and interference that in many cases offers a simple and intuitively transparent understanding of the essence of the proposed high-precision measurements [29].

This review is organized as follows. In the Introduction, we outline the main advanced areas in quantum metrology and sensing which have a significant impact on the development of quantum, information, digital, and other technologies of paramount importance for the modern scientific community. In Section 2, from a unified perspective, we discuss the main goals and objectives of modern quantum metrology, viewed as both a fundamental and applied science of quantum measurements. For clarity, semiclassical methods (based on coherent light) for measuring small phase shifts in optics are presented and the main limitations associated with the SQL are identified. Also in Section 2, we present the fundamentals of a theoretical description of methods and approaches in the language of estimation theory and quantum Fisher information, which have recently become standard in assessing the (maximum permissible) metrological accuracy of a measurement, including with various nonclassical states of the light field discussed in what follows. A related discussion in Section 3 concerns practical issues of the generation and detection of squeezed states of light, which are typically described by continuous variables (CVs) of quantized light radiation, and the so-called $N00N$ states maximally entangled with respect to spatial modes, for which the minimum allowed error in measuring and estimating an unknown phase parameter is predicted theoretically. Such an error can be revealed in an experiment based on the detection of the photon-number parity, which can be done using modern detectors with a photon-number resolution, already making such states practically useful right now. The main emphasis in Section 4 is on the preparation of $N00N$ states and their use in quantum metrology and sensing. Spontaneous parametric down conversion (SPDC) is currently the main resource of modern optical quantum technologies. It is therefore no coincidence that a special place in this review is given to the use of quantum properties of SPDC, which can manifest themselves in the effect of squeezing the dispersion of the quadrature component fluctuations of an optical CV state as well as in the Hong–Ou–Mandel effect for a biphoton. Modern achievements and problems of quantum sensing with $N00N$ states obtained with SPDC are discussed. Section 5 is devoted to the actual capabilities of the quantum metrology schemes considered in this review, with the photon losses, inevitable in practice, taken into account. In this regard, a universal method of fictitious beamsplitters is discussed, which allows revealing the accuracy of measurements and estimates of unknown phase parameters with photon losses taken into account. In Section 6, we identify current problems of quantum photometry, radiometry, and sensing with SPDC based on the schemes of absolute calibration of modern photodetectors as well as frameworks for measuring and assessing temperature with vacuum fluctuations used as a light brightness reference in metrology. In the Conclusions, we summarize the methods and approaches of modern quantum metrology and sensing discussed in the review, which allow practical demonstrations of the 'quantum supremacy' of nonclassical states of light compared to classical ones. Current tasks and development paths for the near future of quantum metrology and sensing are also outlined.

2. Physical foundations of optical quantum metrology

2.1 Quantum metrology. Main goals and objectives

The goal of physical quantum metrology is to develop methods and approaches and to fabricate appropriate instruments and devices that measure physical quantities at the level of quantum limits set by quantum mechanics. We assume that, in the most general case, we have some a priori unknown parameter ϕ, which is to be estimated by quantum metrology methods. The general strategy to do so is a three-step procedure: preparation, measurement, and subsequent statistical evaluation. The quantum metrology algorithm formally presented in Fig. 2 is universal and currently well established (all classical (technological) noise in the system is assumed to be suppressed and decoherence is assumed to be absent; cf. [60]).

At the first stage, as can be seen from Fig. 2a, a probe quantum state $|\psi_{\text{in}}\rangle$ of the light field is prepared. Subsequently, the probe state is subjected to the action of a unitary transformation, which already contains an unknown parameter ϕ, giving rise to the state $|\psi_{\text{out}}\rangle = \hat{U}_\phi|\psi_{\text{in}}\rangle$, where $\hat{U}_\phi$ is the operator of evolution containing information about the unknown parameter ϕ.

The practical implementation of quantum metrology is shown in Fig. 2b, where an MZI is used to prepare $|\psi_{\text{out}}\rangle$. We note that the MZI is physically entirely similar to the MI (cf. Fig. 1). The difference between these interferometers is only in construction: in the MZI, optical beams generally pass through two different beamsplitters BS_1 and BS_2, whereas, in the MI, beams pass twice through the same beamsplitter BS: at the entrance to and at the exit from the interferometer. For this reason, the use of an MI is preferable in practice (it does not require calibrating the relative position of the beamsplitters) [18, 61]. An MZI is more convenient for theoretical research and in quantum technology applications when fabricating photonic chips with modern methods of integrated optics [62]. The MZI theory allows visualizing the evolution of the quantum state of a two-mode system in the Schrödinger picture, or, equivalently, the evolution of the operators in the Heisenberg picture.

Thus, the main problems of optical quantum metrology can be formulated as follows:

• What probe quantum state $|\psi_{\text{in}}\rangle$ can be used for optical quantum metrology?

• What should the transformation $\hat{U}_\phi$ be to yield an estimate of an unknown (small) parameter ϕ with the minimum possible uncertainty?

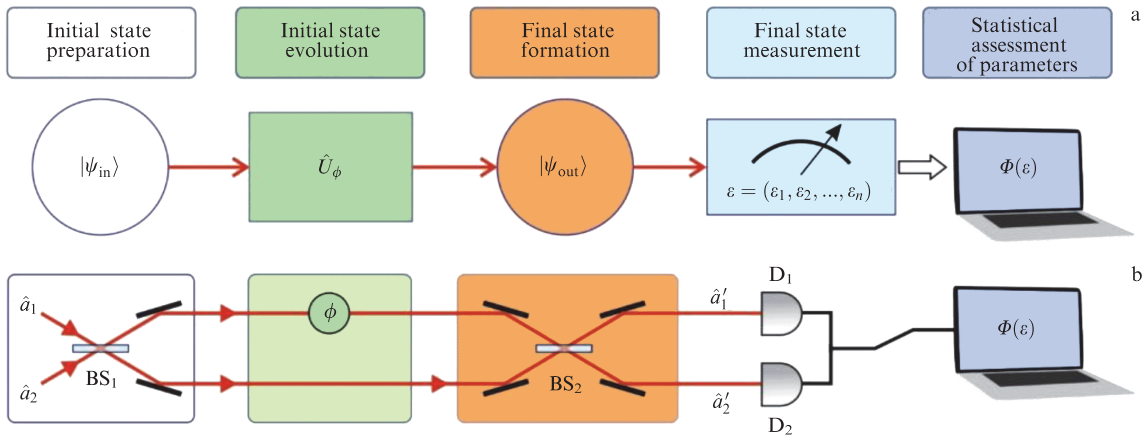

Figure 2. (a) Outline of optical metrology setup to measure and assess unknown phase parameter ϕ based on a step-by-step transformation of initial quantum state $|\psi_{in}\rangle$ of the system and detection of its final state $|\psi_{out}\rangle = \hat{U}_\phi|\psi_{in}\rangle$ in the two-mode approximation. ε are measurement outcomes, $\Phi(\varepsilon)$ is statistical point estimate of unknown parameter ϕ. (b) Optical MZI implementing such a measurement. $\hat{a}_1$, $\hat{a}_2$ and $\hat{a}_1'$, $\hat{a}_2'$ are field modes at entrance to and exit from MZI, $D_{1,2}$ are detectors, and $BS_{1,2}$ are semitransparent beamsplitters.

• How is a point estimate made of an unknown parameter based on measurement outcomes, and how does the estimate of an unknown parameter ϕ depend on the measurement of the $|\psi_{out}\rangle$ state?

We attempt to answer these (and related) questions in this review based on the existing realities and advances in both theory and experiment. We note that various aspects of quantum interference and its use in quantum metrology problems and quantum information processing are also discussed in review [63].

2.2 Elements of the estimation theory for an unknown parameter in quantum mechanics

We begin the discussion of optical quantum metrology methods by answering the third question in Section 2.1. We consider the problem of estimating one unknown physical parameter of the system ϕ by using an already prepared probe state, described by a density operator $\hat{\rho}$, and assume that the parameterization of this probe state $\hat{\rho}_\phi \equiv \hat{U}_\phi \hat{\rho} \hat{U}_\phi^\dagger$ has already been chosen. We only note that, in general, state parameterization can be realized by using a quantum operation that is not necessarily unitary. Measuring the parameterized probe state $\hat{\rho}_\phi$ allows obtaining a set of measurement outcomes to be used to derive an estimate $\tilde{\phi}$ of the unknown parameter ϕ in accordance with some rule. Naturally, in the general case, such an estimate cannot be accurate, $\tilde{\phi} \neq \phi$, and the difference $|\tilde{\phi} - \phi|$ between the point estimate and the unknown parameter determines the accuracy of the procedure used. In addition to this value, the resulting estimate is also assigned some uncertainty. The error of the measurement result is fundamental and is related to Heisenberg's uncertainty relation, which for a quantum mechanical particle has the form

$$\Delta q^2 \Delta p^2 \geqslant \frac{\hbar^2}{4}\,, \tag{2.1}$$

where $\Delta q^2 \equiv \langle(\Delta\hat{q})^2\rangle$ and $\Delta p^2 \equiv \langle(\Delta\hat{p})^2\rangle$ are dispersions of the coordinate and momentum of a particle, characterizing the uncertainty of its physical state in phase space [12]. Thus, we are interested in the problem of finding the minimum uncertainty of the estimated quantity ϕ and the conditions under which it is attained. We note that there are different methods of post-measurement processing of the measurement outcomes ε, implemented using an estimator — a function $\Phi(\varepsilon)$. Various aspects of the choice of the estimator are a subject of mathematical statistics and therefore are not considered here in detail. We only note that the maximum likelihood function method is often used in optical quantum metrology; in what follows, just this function is used as $\Phi(\varepsilon)$. In some cases, the use of the maximum likelihood function method allows obtaining an analytic expression for the estimate $\tilde{\phi}$ and its standard deviation depending on the measurement outcomes.

The analysis outlined in what follows is applicable to various physical systems, including optical media. To extract conditional information from a pre-prepared state $\hat{\rho}_\phi$, we consider a quantum measurement determined by the set of its positive operators $\hat{\Pi}(\varepsilon_i) \geqslant 0$, the so-called POVM (positive operator-valued measure) elements, which satisfy the normalization condition $\sum_{i=1}^m \hat{\Pi}(\varepsilon_i) = \hat{\mathbf{I}}$, where $\hat{\mathbf{I}}$ is the unit operator and ε_i is a set of measurement outcomes (for simplicity, we consider a discrete set of ε_i values; in general, this consideration also applies to the case where ε takes continuous values). Then, the conditional probability can be evaluated as

$$P(\varepsilon_i|\phi) = \mathrm{tr}\left(\hat{\Pi}(\varepsilon_i)\hat{\rho}_\phi\right). \tag{2.2}$$

If the initial state consists of v uncorrelated subsystems, $\hat{\rho}_\phi = \hat{\rho}_\phi^{(1)} \otimes \hat{\rho}_\phi^{(2)} \otimes \ldots \otimes \hat{\rho}_\phi^{(v)}$, with the same parameterization, then the conditional probability of a given separable v-partite state is $P^{(v)}(\varepsilon_i|\phi) = \prod_{i=1}^v P(\varepsilon_i|\phi)$.

We consider the case of one measurement with a measurement result ε, which allows the experimenter to obtain an estimate $\Phi(\varepsilon) = \tilde{\phi}$ and assign it to the unknown parameter ϕ. But this estimate can only be correct on average,

$$\langle\Phi\rangle = \sum_i \Phi(\varepsilon_i)\, P(\varepsilon_i|\phi)\,, \tag{2.3}$$

when the measurement of identically prepared states is repeated a large number of times with an unbiased estimator $\langle\Phi\rangle = \phi$. Information on the uncertainty in estimating the unknown parameter ϕ is contained in the dispersion of the

estimator, which can be standardly evaluated as

$$\langle \Delta\Phi^2 \rangle \equiv \Delta\Phi^2 = \sum_i \big(\Phi(\varepsilon_i) - \langle\Phi\rangle\big)^2 P(\varepsilon_i|\phi)\,. \tag{2.4}$$

The quantities $\langle\Phi\rangle$ and $\langle\Delta\Phi^2\rangle$ can depend on ϕ, but we omit their argument. The tools of mathematical statistics allow estimating the lower limit of the estimator dispersion. Remarkably, the boundary value can be obtained via simple algebraic transformations. For this, we use two quantities: the derivative of the average of the statistical estimate $\partial\langle\Phi\rangle/\partial\phi = \langle\Phi\,\partial L(\varepsilon_i|\phi)/\partial\phi\rangle$, where $L(\varepsilon_i|\phi) = \ln P(\varepsilon_i|\phi)$ is the logarithmic conditional probability [60], and the averaged logarithmic derivative $\langle\partial L/\partial\phi\rangle = 0$. With the Cauchy–Schwarz inequality for operators $\langle \hat{A}\,\hat{B}\rangle^2 \leqslant \langle\hat{A}^2\rangle\langle\hat{B}^2\rangle$, the chain of transformations

$$\begin{aligned}\left(\frac{\mathrm{d}\langle\Phi\rangle}{\mathrm{d}\phi}\right)^2 &= \left(\left\langle \Phi\,\frac{\partial L}{\partial\phi} - \langle\Phi\rangle\,\frac{\partial L}{\partial\phi}\right\rangle\right)^2 \\ &= \left(\left\langle \big(\Phi - \langle\Phi\rangle\big)\,\frac{\partial L}{\partial\phi}\right\rangle\right)^2 \leqslant \left\langle \big(\Phi - \langle\Phi\rangle\big)^2\right\rangle\left\langle\left(\frac{\partial L}{\partial\phi}\right)^2\right\rangle \\ &= \Delta\Phi^2\,F(\phi)\end{aligned} \tag{2.5}$$

allows estimating the lower bound (the Cramér–Rao bound, CRB) of the standard deviation of the estimator $\Delta\Phi_{\mathrm{CR}}$ for the obtained probability distribution (2.2),

$$\Delta\Phi \geqslant \Delta\Phi_{\mathrm{CR}} = \frac{1}{\sqrt{F(\phi)}}\,\frac{\mathrm{d}\langle\Phi\rangle}{\mathrm{d}\phi}\,, \tag{2.6}$$

where we use the expression for Fisher information

$$F(\phi) = \left\langle\left(\frac{\partial L}{\partial\phi}\right)^2\right\rangle = \sum_i \frac{1}{P(\varepsilon_i|\phi)}\left(\frac{\mathrm{d}P(\varepsilon_i|\phi)}{\mathrm{d}\phi}\right)^2. \tag{2.7}$$

In the case of an unbiased estimator ($\mathrm{d}\langle\Phi\rangle/\mathrm{d}\phi = 1$), we obtain the expression for the CRB widely used in the literature (see, e.g., [11, 60, 64]),

$$\Delta\Phi_{\mathrm{CR}} = \frac{1}{\sqrt{\nu F(\phi)}}\,, \tag{2.8}$$

for a separable state $\hat{\rho}_\phi$ with a set of measurement outcomes $\varepsilon = (\varepsilon_1, \varepsilon_2, \ldots, \varepsilon_\nu)$, because Fisher information becomes an additive quantity in this case, $F_\nu = \nu F$. We note that (2.8) follows from the theorem on the asymptotic attainability of the CRB in the case where the maximum likelihood method is used for the estimator $\Phi(\varepsilon)$. It can be proved that, in the limit of $\nu \to \infty$ measurement outcomes, the asymptotic distribution $\Phi(\varepsilon)$ is Gaussian with the mean ϕ and dispersion $1/\nu F(\phi)$, which can be conventionally represented as $\Phi(\varepsilon) \sim P_n(\phi, 1/\nu F(\phi))$, where P_n is the standard Gaussian distribution and the symbol $\sim$ is used in the sense that the asymptotic distribution $\Phi(\varepsilon)$ approaches the Gaussian distribution as $\nu \to \infty$.

The family of measurements with a set of measuring elements $\{\Pi(\varepsilon_i)\}$ is infinite, which gives rise to the problem of maximizing Fisher information by seeking a measurement that maximizes the Fisher information of the $\hat{\rho}_\phi$ state used, i.e., $F_q(\phi) = \max_{\{\Pi(\varepsilon_i)\}} F(\phi)$; this quantity is called the quantum Fisher information (QFI). It can be shown that the procedure for maximizing with respect to the measuring elements leads to a decrease in the lower bound for the unknown parameter estimates to its ultimate fundamental limit $\Delta\Phi_{\mathrm{QCR}}$ (the quantum Cramér–Rao bound, QCRB) and, in the case of an unbiased estimator, the following inequalities hold:

$$\Delta\Phi \geqslant \Delta\Phi_{\mathrm{CR}} \geqslant \Delta\Phi_{\mathrm{QCR}} = \frac{1}{\sqrt{\nu F_q(\phi)}}\,. \tag{2.9}$$

Thus, a fundamental problem in quantum metrology and sensing is to find the QFI $F_q(\phi)$, which is directly related to the procedure for measuring the unknown parameter ϕ and its dispersion. Below, we discuss the physical quantum metrology schemes where $F_q(\phi)$ can be maximized.

The QFI F_q, in turn, is the dispersion of the Hermitian operator of the symmetric logarithmic derivative $F_q(\phi) = \Delta D^2 = \mathrm{tr}\,(\hat{\rho}_\phi\hat{D}^2)$, because $\langle\hat{D}\rangle = \mathrm{tr}\,(\hat{\rho}_\phi\hat{D}) = 0$. This operator satisfies the equation $\mathrm{d}\hat{\rho}_\phi/\mathrm{d}\phi = (\hat{\rho}_\phi\hat{D} + \hat{D}\hat{\rho}_\phi)/2 = \{\hat{\rho}_\phi\hat{D}\}/2$, where $\{\hat{A}, \hat{B}\} = \hat{A}\hat{B} + \hat{B}\hat{A}$ is the anticommutator of two operators. The solution of this equation, realized by diagonalizing the initial state to $\hat{\rho}_\phi = \sum_i \lambda_i|\psi_i\rangle\langle\psi_i|$, always exists: $\hat{D} = 2\sum_{ij}\{\hat{\rho}_\phi\hat{D}\}_{ij}|\psi_i\rangle\langle\psi_j|/(\lambda_i + \lambda_j)$. This allows calculating the quantum limit of Fisher information as

$$\begin{aligned}F_q(\hat{\rho}_\phi) = \mathrm{tr}\,(\hat{\rho}_\phi\hat{D}^2) &= \sum_i \frac{(\partial_\phi\lambda_i)^2}{\lambda_i} \\ &+ 2\sum_{i,j}\frac{(\lambda_i - \lambda_j)^2}{\lambda_i + \lambda_j}\,\big|\langle\partial_\phi\psi_i|\psi_j\rangle\big|^2\,.\end{aligned} \tag{2.10}$$

Here and hereafter, ∂_ϕ denotes the derivative of a function or state with respect to the parameter ϕ. The QFI no longer depends on the type of measurement chosen and is completely determined by the probe state $\hat{\rho}_\phi$. Knowing the form of the symmetric logarithmic derivative operator, we can choose the eigenstates of this operator $\hat{D} = \sum_i \lambda_i^{(D)}|\psi_i^{(D)}\rangle\langle\psi_i^{(D)}|$, which can also depend on ϕ, as the measuring elements $\{\Pi(\varepsilon_i) = |\psi_i^{(D)}\rangle\langle\psi_i^{(D)}|\}$, thereby reducing the uncertainty of the estimator to the QCRB value. We note that the choice of eigenstates of $\hat{D}$ is not the only POVM measurement that allows attaining the QCRB, but the search for such operators is a difficult problem in general. A situation is possible in which the experimenter can surmise what values the unknown parameter ϕ can take as a result of preliminary 'rough' measurements in order to 'improve' the measurement basis of the subsequent measurements, but such complex adaptive strategies are beyond the scope of this review. The expression for the QFI in (2.10) can depend on ϕ in a rather intricate way, and therefore the choice of the probe state $\hat{\rho}_\phi$ can be good in a certain range of ϕ values. Conversely, the use of the same state $\hat{\rho}_\phi$ does not guarantee that this state can be useful in estimating ϕ in another range.

Calculating the QFI in (2.10) may turn into a rather involved technical problem, which, however, can be simplified in two common cases. For example, the form of the symmetric logarithmic derivative operator is simplified to $\hat{D} = 2\partial_\phi\hat{\rho}_\phi$ in the case of a pure state $\hat{\rho}_\phi = |\psi_{\mathrm{out}}\rangle\langle\psi_{\mathrm{out}}|$, which can be proved directly starting with the definition of the operator $\hat{D}$ and the condition $\hat{\rho}_\phi = \hat{\rho}_\phi^2$ for pure states. The pure-state QFI then becomes

$$F(\psi_{\mathrm{out}}) = 4\Big(\langle\partial_\phi\psi_{\mathrm{out}}|\partial_\phi\psi_{\mathrm{out}}\rangle - \big|\langle\partial_\phi\psi_{\mathrm{out}}|\psi_{\mathrm{out}}\rangle\big|^2\Big)\,, \tag{2.11}$$

which is most often taken as the definition of QFI in modern scientific literature [11, 60, 64].

The second assumption, which partly answers the second question, is the possibility of a unitary 'encoding' of the probe state

$$\hat{U}_\phi = \exp\left(-\mathrm{i}\phi\hat{G}\right) \tag{2.12}$$

with a Hermitian generator $\hat{G}$ (cf. [64]). The operator $\hat{U}_\phi$ defines a transformation of the pure state $|\psi_{\text{out}}\rangle = \hat{U}_\phi|\psi_{\text{in}}\rangle$, and, in the general case, of a mixed probe state $\hat{\rho}_\phi = \hat{U}_\phi\hat{\rho}\hat{U}_\phi^\dagger$, and satisfies the von Neumann equation $\mathrm{i}\,\partial\hat{\rho}_\phi/\partial\phi = [\hat{G}, \hat{\rho}_\phi]$, where $[\hat{A}, \hat{B}] = \hat{A}\hat{B} - \hat{B}\hat{A}$ is the commutator of two operators. Thus, the QFI can be calculated as four times the dispersion of the observable $\hat{G}$:

$$F_q(\psi_{\text{out}}, \hat{G}) = 4\left(\langle\hat{G}^2\rangle - |\langle\hat{G}\rangle|^2\right) \equiv 4\Delta G^2 \tag{2.13}$$

for a pure state and

$$F_q(\hat{\rho}_\phi, \hat{G}) = 2\sum_{i,j}\frac{(\lambda_i - \lambda_j)^2}{\lambda_i + \lambda_j}\left|\langle\psi_i|\hat{G}|\psi_j\rangle\right|^2 \tag{2.14}$$

for a mixed state $\hat{\rho}_\phi$ in the most common case $\partial_\phi\lambda_i = 0$, when the classical contribution $\hat{\rho}_\phi$ to this quantity is not used. Expression (2.14) may seem weird when trying to use it, e.g., for a pure state or a balanced state with $\lambda_1 = \lambda_2 = \ldots \lambda_i = 1/N$. The 'weirdness' entirely disappears when using the completeness of the basis states $|\psi_i\rangle$ together with two obvious transformations, $(\lambda_i - \lambda_j)^2 = (\lambda_i + \lambda_j)^2 - 4\lambda_i\lambda_j$ and $\langle\partial_\phi\psi_i|\psi_j\rangle = -\langle\psi_i|\partial_\phi\psi_j\rangle$, which allows writing (2.14) in the form

$$F_q(\hat{\rho}_\phi, \hat{G}) = 4\left(\sum_i \lambda_i\langle\psi_i|\hat{G}^2|\psi_i\rangle - 2\sum_{i,j}\frac{\lambda_i\lambda_j}{\lambda_i + \lambda_j}\left|\langle\psi_i|\hat{G}|\psi_j\rangle\right|^2\right). \tag{2.15}$$

We also note the important convexity and additivity properties of QFI,

$$F_q\left(\hat{\rho}_\phi = \sum_i \lambda_i\hat{\rho}_\phi^{(i)}\right) \leqslant \sum_i \lambda_i F_q\left(\hat{\rho}_\phi^{(i)}\right), \tag{2.16}$$

$$F_q\left(\otimes\hat{\rho}_\phi^{(i)}\right) \leqslant \sum_i F_q\left(\hat{\rho}_\phi^{(i)}\right), \tag{2.17}$$

and the inequality

$$F_q(\hat{\rho}_\phi, \hat{G}) \leqslant 4\Delta G^2, \tag{2.18}$$

which can be qualitatively explained as follows: adding classical information to the formation of a mixed state $\hat{\rho}_\phi$ reduces the total amount of information that can be gleaned from measuring the state. The last step to determine the exact bound for the unknown parameter is to maximize the QFI in (2.15) with respect to the probe states, i.e., to seek a state $\hat{\rho}$ that provides the maximum QFI, $\max_{\hat{\rho}_\phi} F(\hat{\rho}_\phi)$, which is already beyond the scope of this review but is touched upon in some examples below.

Estimates (2.13) and (2.14) were obtained with the use of a generator $\hat{G}$ of the physical system. We therefore consider the case, important in practice, of estimating a physically small parameter ϕ. In this limit, the parameter uncertainty $\Delta\phi \ll 1$ can be estimated based on the error propagation formula [11, 64]

$$\Delta\phi = \frac{\Delta I}{\partial I/\partial\phi}, \tag{2.19}$$

which involves the standard deviation $\Delta I \equiv (\langle\hat{I}^2\rangle - \langle\hat{I}\rangle^2)^{1/2}$ and the average $I = \langle\hat{I}\rangle$ of the operator of a detected (random) signal $\hat{I}$. As can be seen from (2.19), assuming all other conditions to be ideal, increasing the accuracy of measuring small displacements requires, first, an increase in the signal-to-noise ratio and, second, the maximum slope of the curve, determined by $\partial I/\partial\phi$. A decrease in ΔI is possible to the shot noise level [65], due to the efficiency of signal detectors. This noise determines the SQL of classical measurements.

The smallness condition $\phi \ll 1$ allows approximating the transformation of the operator of the observable $\hat{I}' = \hat{U}_\phi^\dagger\hat{I}\hat{U}_\phi$ as

$$\hat{I}' = \exp\left(\mathrm{i}\phi\hat{G}\right)\hat{I}\exp\left(-\mathrm{i}\phi\hat{G}\right) \approx \hat{I} - \mathrm{i}\phi[\hat{I}, \hat{G}]. \tag{2.20}$$

For any two operators $\hat{I}$ and $\hat{G}$, we can write the uncertainty relation in the form

$$\Delta I\Delta G \geqslant \frac{1}{2}\left|[\hat{I}, \hat{G}]\right|, \tag{2.21}$$

and hence the expression for the phase error propagation in (2.19) takes the form

$$\Delta\phi = \frac{\Delta I}{|\partial\langle\hat{I}\rangle/\partial\phi|} = \frac{\Delta I}{\left|[\hat{I}, \hat{G}]\right|} \geqslant \Phi_{\text{QCR}} = \frac{1}{2\Delta G}, \tag{2.22}$$

which coincides with the QCRB in (2.9) and (2.11). In estimation theory, relations (2.22) physically embody the uncertainty principle [64]. Hence, in quantum metrology, the quantity $\Delta\phi$ is to be minimized by choosing the appropriate operator $\hat{G}$ of a physical quantity and the probe quantum state of the light field with respect to which the averaging is done.

2.3 Advantages of nonclassical states in estimating an unknown parameter in linear metrology

We now consider the answer to the first question posed in Section 2.1: the use of nonclassical states of light in optical quantum metrology, which allows researchers to obtain an extra 'quantum' resource that is decisive in ensuring the advantage of quantum technologies over classical ones in ultraprecise estimations of an unknown parameter [66]. Such states are the subject of quantum optics: over the past three decades of development, a significant number of nonclassical states have been presented, and methods for their transformation, preparation, and measurement have been developed [22, 67].

In classical optics, the key parameter is the phase difference, for example, between MZI arms, which determines the interference at the exit (see Fig. 2). The phase difference is regarded as a classical parameter rather than a quantum observable, which leaves this parameter subject to estimates rather than measurements. A detailed discussion of the phase problem in quantum optics, the existence of a Hermitian phase operator of the electromagnetic field, and related detection methods can be found elsewhere (see, e.g., [68, 69]).

In many practically important cases, the phase difference between two light beams whose behavior we observe can be represented as the sum $\phi_0 + \phi$ of a 'classical' part of the phase shift (the reference phase) ϕ_0, which is known a priori from the preparation of the initial quantum state (or from the results of a previous classical measurement), and the

unknown part ϕ. An 'extra' increase in the light wave phase ϕ occurs when one of the MZI arms contains a transparent medium with an unknown refractive index that depends on the material parameters of the medium, temperature, and so on, which are just the ultimate goal of measurement and estimation in metrology and sensing. In that case, the error in measuring the phase difference $\Delta(\phi_0+\phi)=\Delta\phi$ is entirely determined by $\Delta\phi$, whose measurements and estimates are discussed below. The choice of the reference phase ϕ_0 is determined by the condition of minimizing the resultant measurement error. Another example of an unknown parameter that can be estimated by quantum mechanics is provided by the photon delay time τ in the Hong–Ou–Mandel interferometer.

We use expression (2.19) to estimate the uncertainty in measuring the phase difference in the MZI shown in Fig. 2b. In the Heisenberg picture, the input and output channels of the interferometer can be described by the respective bosonic annihilation operators $\hat{a}_1$, $\hat{a}_2$, and $\hat{a}_1'$, $\hat{a}_2'$, which satisfy the standard bosonic commutation relations

$$[\hat{a}_i,\hat{a}_j^\dagger]=[\hat{a}_i',\hat{a}_j'^\dagger]=\delta_{ij}\,. \tag{2.23}$$

Mathematically, the propagation of fields in the MZI can be conveniently represented using the quasispin operators of a two-mode system [70],

$$\begin{aligned}\hat{J}_X&=\frac{1}{2}(\hat{a}_1^\dagger\hat{a}_2+\hat{a}_2^\dagger\hat{a}_1)\,,\\ \hat{J}_Y&=\frac{1}{2\mathrm{i}}(\hat{a}_1^\dagger\hat{a}_2-\hat{a}_2^\dagger\hat{a}_1)\,,\\ \hat{J}_Z&=\frac{1}{2}(\hat{a}_1^\dagger\hat{a}_1-\hat{a}_2^\dagger\hat{a}_2)\,,\end{aligned} \tag{2.24}$$

which satisfy the SU(2) algebra commutation relations

$$[\hat{J}_X,\hat{J}_Y]=\mathrm{i}\hat{J}_Z\,,\qquad [\hat{J}_Y,\hat{J}_Z]=\mathrm{i}\hat{J}_X\,,\qquad [\hat{J}_Z,\hat{J}_X]=\mathrm{i}\hat{J}_Y\,. \tag{2.25}$$

The operation of the MZI can be described as a sequence of rotations in an abstract (spin) space, defined by the unitary operator $\hat{U}_\Theta=\exp(-\mathrm{i}\Theta\hat{\mathbf{J}}\mathbf{n})$ (where $\hat{\mathbf{J}}=\{\hat{J}_X,\hat{J}_Y,\hat{J}_Z\}$ and Θ and $\mathbf{n}$ are the angle and the vector of the rotation axis), similarly to angular momentum in quantum mechanics (see, e.g., [71]). The transformation of quasispin operators in the setup in Fig. 2b can then be written as

$$\hat{J}_j'=\hat{U}_{\mathrm{MZ}}^\dagger\hat{J}_j\hat{U}_{\mathrm{MZ}}\,,\quad j=X,Y,Z\,, \tag{2.26}$$

where the operator

$$\hat{U}_{\mathrm{MZ}}=\hat{U}_{\mathrm{BS}}^\dagger\hat{U}_\phi\hat{U}_{\mathrm{BS}} \tag{2.27}$$

describes the evolution of states in the MZI [11, 70, 72]. In (2.27), $\hat{U}_{\mathrm{BS}}=\exp(-\mathrm{i}(\pi/2)\hat{J}_X)$ is the equilibrium beamsplitter operator, and the evolution operator of the phase parameter has the form

$$\hat{U}_\phi=\exp(-\mathrm{i}\phi\hat{J}_Z)\,. \tag{2.28}$$

It can be shown that, in this configuration, the MZI operator in (2.27) becomes $\hat{U}_{\mathrm{MZ}}=\exp(-\mathrm{i}\phi\hat{J}_Y)$. Detectors at the exit from the MZI measure the photon numbers $\hat{N}_{1,2}^{\mathrm{out}}$, which allow defining a Hermitian observable, the photon-number difference operator $\hat{I}=\hat{N}_2^{\mathrm{out}}-\hat{N}_1^{\mathrm{out}}=\hat{a}_2'^\dagger\hat{a}_2'-\hat{a}_1'^\dagger\hat{a}_1'=-2\hat{J}_Z'$. Thus, the standard deviation

$$\Delta I=2\Delta J_Z'=2\sqrt{\langle\hat{J}_Z'^2\rangle-\langle\hat{J}_Z'\rangle^2}$$

bounds the measurement accuracy of the phase parameter ϕ.

In quantum optics, an interferometer built based on the SU(2) rotation group can easily be implemented using linear optical elements: beamsplitters, phase shifters, and so on (see, e.g., [73]). Based on relations (2.26), the average value of the experimentally measured quantity $\langle\hat{J}_Z'\rangle$ can be expressed in terms of operators (2.24) averaged with respect to the input quantum state $|\psi_{\mathrm{in}}\rangle$:

$$\langle\hat{J}_Z'\rangle=\cos(\phi)\,\langle\hat{J}_Z\rangle_{\mathrm{in}}-\sin(\phi)\,\langle\hat{J}_X\rangle_{\mathrm{in}}\,. \tag{2.29}$$

Calculating $\Delta J_Z'$ leads to an expression for the dispersion $\Delta J_Z'^2$ in the form

$$\Delta J_Z'^2=\cos^2(\phi)\Delta J_Z^2+\sin^2(\phi)\Delta J_X^2-\sin(2\phi)\,\mathrm{cov}\,(\hat{J}_Z,\hat{J}_X)\,, \tag{2.30}$$

where $\mathrm{cov}\,(\hat{J}_Z,\hat{J}_X)$ is the covariance parameter of the operators $\hat{J}_Z$ and $\hat{J}_X$, defined as

$$\mathrm{cov}\,(\hat{J}_Z,\hat{J}_X)=\frac{1}{2}\big\langle(\hat{J}_Z\hat{J}_X+\hat{J}_X\hat{J}_Z)\big\rangle_{\mathrm{in}}-\langle\hat{J}_X\rangle_{\mathrm{in}}\langle\hat{J}_Z\rangle_{\mathrm{in}}\,. \tag{2.31}$$

In the MZI representation, when measuring the observable quantity $I=\langle 2\hat{J}_Z'\rangle$, formula (2.22) becomes

$$\Delta\phi=\frac{\Delta J_Z'^2}{\left|\partial\langle\hat{J}_Z'\rangle/\partial\phi\right|} \tag{2.32}$$

(cf. (2.19)).

Let us consider specific examples. In the semiclassical limit, coherent (laser) radiation is supplied to input 1, and input 2 is left 'idle,' i.e., in the vacuum state, and hence $|\psi_{\mathrm{in}}\rangle=|\alpha\rangle_1|0\rangle_2\equiv|\alpha,0\rangle$, where $|0\rangle$ is the vacuum state and

$$|\alpha\rangle=\exp\left(-\frac{|\alpha|^2}{2}\right)\sum_{n=0}^{\infty}\frac{\alpha^n}{\sqrt{n!}}\,|n\rangle \tag{2.33}$$

is a coherent state ($|\alpha|^2=\langle\hat{N}\rangle\equiv N$ is the average number of photons in the interferometer). From (2.32), we then obtain

$$\Delta\phi=\frac{1}{\sqrt{N}\,|\sin(\phi)|}\,. \tag{2.34}$$

Expression (2.34) can be optimized near the value of the reference phase $\phi\simeq\phi_0=\pi/2$, which gives the following estimate for coherent states:

$$\Delta\phi_{\mathrm{coh}}=\frac{1}{\sqrt{N}}\equiv\Delta\phi_{\mathrm{SQL}}\,. \tag{2.35}$$

The value in (2.35) determines the SQL in quantum metrology measurements, also known experimentally as the shot noise limit [14]. Physically, this is the ultimate accuracy of classical interferometry, which involves coherent sources of laser radiation with $|\alpha|^2\gg1$, assuming the complete absence of radiation losses in the MZI. To overcome the SQL in (2.35), essentially nonclassical quantum states must be used, which are discussed in what follows. Before that, we note that the same result (2.35) can be obtained from (2.18) in the form $\Delta\phi_{\mathrm{coh}}=1/2\Delta\hat{J}_Z)$, because $\Delta\hat{J}_Z=(1/2)|\alpha|=(1/2)\sqrt{N}$ for the state in (2.33).

We next consider classical single-mode states $\hat{\rho}_{\rm cl} = \int d^2\alpha\, P_{\rm cl}(\alpha)|\alpha\rangle\langle\alpha|$, where the Glauber–Sudarshan quasidistribution $P_{\rm cl}(\alpha)$ is a classical probability density, $P_{\rm cl}(\alpha) \geqslant 0$. Using inequality (2.18), we can then estimate the QFI for the generator $\hat{G} \equiv \hat{N}/2 = \hat{a}^\dagger\hat{a}/2$ as

$$F_q\left(\hat{\rho}_{\rm cl}, \frac{\hat{N}}{2}\right) \leqslant \Delta\hat{N}_{\rm cl}^2 = \int d^2\alpha\, P_{\rm cl}(\alpha)|\alpha|^2 = {\rm Tr}\,(\hat{\rho}_{\rm cl}\hat{N}) = N_{\rm cl}\,. \tag{2.36}$$

Expression (2.36) implies a lower bound for the standard deviation of the phase when measuring a classical state in one dimension $v = 1$:

$$\Delta\phi_{\rm QCR} \geqslant \frac{1}{\sqrt{N_{\rm cl}}}\,. \tag{2.37}$$

To obtain a lower value of the uncertainty of $\Delta\phi_{\rm QCR}$, we have to ensure the condition $F_q(\hat{\rho}, \hat{N}/2) > N_\rho$. Therefore, the measured state $\hat{\rho}$ must be nonclassical, which in combination with inequality (2.18) allows obtaining the necessary (although not sufficient) condition $\Delta N_\rho^2 > N_\rho$ for the SQL to be overcome. Interestingly, the required nonclassical state $\hat{\rho}$ must a have super-Poisson statistics to satisfy condition (2.37), which means that not every nonclassical state can be useful in optical quantum metrology.

Next, as examples of nonclassical states, we consider a single-mode squeezed vacuum (SMSV) state with a real value of the squeezing parameter of the quadrature component $r > 0$, which we represent in the form

$$\left|{\rm SMSV}(y)\right\rangle = \frac{1}{\sqrt{\cosh(r)}} \sum_{n=0}^{\infty} \frac{y^n}{\sqrt{(2n)!}} \frac{(2n)!}{n!}|2n\rangle\,, \tag{2.38}$$

where $y = \tanh(r)/2$. If we pass this state through a beamsplitter with arbitrary real transmission, T, and reflection, R, amplitudes, then the output state becomes a hybrid entangled state [74, 75]

$$BS_{12}\left(|{\rm SMSV}(y)\rangle_1|0\rangle_2\right) = \frac{1}{\sqrt{\cosh(r)}} \sum_{l=0}^{\infty} c_l^{(0)}(y_1, B)\sqrt{Z^{(l)}(y_1)}\,\left|\Psi_l^{(0)}(y_1)\right\rangle_1|l\rangle_2 \tag{2.39}$$

with the amplitudes $c_l^{(0)}(y_1, B) = (-1)^l(y_1 B)^{l/2}/\sqrt{l!}$, where the input squeezing parameter y becomes equal to $y_1 = yT^2 = y/(1+B) \leqslant y$ with the beamsplitter parameter $B = (1-T^2)/T^2$; also, $Z^{(n)}(y_1) = d^n Z(y_1)/dy_1^n$ is the nth derivative of the function $Z(y_1) = 1/(1-4y_1^2)^{1/2}$ with $n = 2m, 2m+1$. Definite-parity states are defined as

$$\left|\Psi_{2m}(y_1)\right\rangle = \frac{1}{\sqrt{Z^{(2m)}(y_1)}} \sum_{n=0}^{\infty} \frac{y_1^n}{\sqrt{(2n)!}} \frac{\left(2(n+m)\right)!}{(n+m)!}|2n\rangle\,, \tag{2.40}$$

$$\left|\Psi_{2m+1}(y_1)\right\rangle = \sqrt{\frac{y_1}{Z^{(2m+1)}}} \sum_{n=0}^{\infty} \frac{y_1^n}{\sqrt{(2n+1)!}} \times \frac{\left(2(n+m+1)\right)!}{(n+m+1)!}|2n+1\rangle \tag{2.41}$$

and are obtained from hybrid entangled state (2.39) by extracting $2m$ and $2m+1$ photons from it.

Hybrid state (2.39) and so-called measurement-induced states, both even (Eqn (2.40)) and odd (Eqn (2.41)), are based on the preparation of the required state by measurements carried out on a 'part' of the state obtained within the scheme (cf. [76]) and are of significant interest for optical quantum metrology; the measurement-induced preparation of the $N00N$ state is to be discussed in Section 4.4. An increase in the number of extracted photons leads to a significant increase in the average number of particles in measurement-induced states, which allows obtaining a lower uncertainty of the estimated parameter compared with the uncertainty provided by the initial state (2.38) [75]. In addition, measurement-induced states (2.40) and (2.41) can be approximated as even,

$$\left|{\rm SCS}_+(\alpha)\right\rangle = 2N_+(\alpha)\exp\left(-\frac{|\alpha|^2}{2}\right)\sum_{n=0}^{\infty}\frac{\alpha^{2n}}{\sqrt{(2n)!}}\,|2n\rangle\,, \tag{2.42}$$

and odd,

$$\left|{\rm SCS}_-(\alpha)\right\rangle = 2N_-(\alpha)\exp\left(-\frac{|\alpha|^2}{2}\right)\sum_{n=0}^{\infty}\frac{\alpha^{2n+1}}{\sqrt{(2n+1)!}}\,|2n+1\rangle\,, \tag{2.43}$$

optical Schrödinger-cat states; they have the amplitude $\alpha > 5$ with an accuracy greater than 0.99, where $N_\pm(\alpha) = 1/[2(1 \pm \exp(-2|\alpha|^2))]^{1/2}$ is the normalization coefficient [74]. Optical Schrödinger-cat states are another example of states with a continuous observable that can be used in optical quantum metrology.

Among two-mode states, the maximally entangled state

$$|N00N\rangle = \frac{1}{\sqrt{2}}\left(|N, 0\rangle + |0, N\rangle\right) \tag{2.44}$$

plays an important role in quantum metrology, as do various types of separable states composed of the above single-mode states. For example, we can use the separable state $|{\rm SMSV}\rangle_1|n\rangle_2$ at the entrance to the MZI, where the number n can take values $n = 0$ and $n \neq 0$. The input state can also be an arbitrary mixture of a coherent or a thermal state with the photon state $\hat{\rho} = \hat{\rho}_a \otimes |N\rangle_b\langle N|$ [77]. The use of entangled states at the entrance to the MZI can provide an additional resource for ultraprecise estimates of an unknown parameter.

Table 1 shows analytic expressions for quantum Fisher information for some selected states when using the generator $\hat{G} \equiv \hat{J}_Z$ with the input state $|\psi_{\rm in}\rangle_1|0\rangle_2$, which transforms into $|\psi_{\rm out}\rangle = \hat{U}_\phi|\psi_{\rm in}\rangle_1|0\rangle_2 = \exp(-i\phi\hat{J}_Z)|\psi_{\rm in}\rangle_1|0\rangle_2$. As we can see from the table, only the Fock state and the odd Schrödinger-cat state cannot overcome the SQL. Moreover, a single-mode squeezed vacuum state can also overcome the Heisenberg limit, to be discussed below, because $\Delta n_{\rm SMSV}^2 \geqslant \langle n\rangle_{\rm SMSV}^2$. For the Schrödinger-cat states, on the other hand, the term $\propto |\alpha|^4$ is a correction that vanishes for $N \gg 1$. Although nonclassical states of light can overcome the SQL, realizing this advantage in practice is a challenging experimental task, which faces obstructions due to the level of development of modern quantum optical technologies (as we discuss in subsequent sections).

Interestingly, in the context of metrological applications, so-called *four-mode* scalar light, whose polarization degree is zero, may be of some interest, because the total averages of the Stokes operators are also equal to zero [77]. However, the issue of their use in quantum metrology problems requires separate studies that go beyond the scope of this review.

Table 1. Quantum Fisher information of some nonclassical and coherent states in the case where phase shift operators $\hat{U}_\phi = \exp(-\mathrm{i}\phi\hat{J}_Z)$ are applied to initial (probe) pure state $|\psi_{\mathrm{in}}\rangle$, i.e., $|\psi_{\mathrm{out}}\rangle = \hat{U}_\phi|\psi_{\mathrm{in}}\rangle$ or $|\psi_{\mathrm{out}}\rangle = \hat{U}_\phi|\psi_{\mathrm{in}}\rangle \otimes |0\rangle$. Some estimates are expressed in units of average number of particles $N \equiv \langle\hat{N}\rangle$ for convenience.

Probe state $\lvert\psi_{\mathrm{in}}\rangle$	Average number of particles $\langle\hat{N}\rangle \equiv N$	Quantum Fisher information, $F_q(\psi_\phi, \hat{G}) \equiv 4\Delta G^2$, $\hat{G} \equiv \hat{J}_Z$
Fock state $\lvert N\rangle$	N	0
Coherent state $\lvert\alpha\rangle$	$\lvert\alpha\rvert^2$	N
Single-mode squeezed vacuum state $\lvert\mathrm{SMSV}\rangle$	$\sinh^2(r)$	$2(N^2+N)$
$N00N$ state $\lvert N00N\rangle$	N	N^2
Even Schrödinger-cat state $\lvert\mathrm{SCS}_+(\alpha)\rangle$	$\lvert\alpha\rvert^2\tanh(\lvert\alpha\rvert^2)$	$N + \dfrac{\lvert\alpha\rvert^4}{\cosh^2(\lvert\alpha\rvert^2)}$
Odd Schrödinger-cat state $\lvert\mathrm{SCS}_-(\alpha)\rangle$	$\lvert\alpha\rvert^2\coth(\lvert\alpha\rvert^2)$	$N - \dfrac{\lvert\alpha\rvert^4}{\sinh^2(\lvert\alpha\rvert^2)}$

2.4 Limit estimates of phase parameters in nonlinear metrology

We have tacitly assumed in the foregoing that the phase ϕ is independent of the number of particles. But, in a more general formulation of the problem, ϕ should be considered a small parameter dependent on the number of photons. Physically, this situation may correspond, for example, to measuring and estimating the cubic nonlinearity parameter of a transparent medium placed in one of the MZI arms and causing an additional nonlinear phase shift.

Because the calculation of the lower CRB in this case is an ongoing problem in modern quantum theory, we present only limit estimates of the accuracy of measuring phase parameters, derivable by intuitively relying on the use of nonclassical states, which are useful in linear metrology. We therefore consider generators of two types: those corresponding to linear (separable) and to nonlinear (nonseparable) transformations. These generators can be respectively represented as the sum $\hat{G}_{\mathrm{L}} = \sum_{i=1}^{k}\hat{g}_i$ and the product $\hat{G}_{\mathrm{NL}} = \prod_{i=1}^{k}\hat{g}_i$ of k generators. The dispersions of such generators can be represented in the form [79, 80]

$$\Delta G_{\mathrm{L}} = \frac{k}{2}(\lambda_{\max} - \lambda_{\min}), \quad \Delta G_{\mathrm{NL}} = \frac{1}{2}(\lambda_{\max}^k - \lambda_{\min}^k), \quad (2.45)$$

where $\lambda_{\max}$ and $\lambda_{\min}$ are the maximum and minimum eigenvalues of $\hat{g}_i$. Because the $\hat{g}_i$ are most often taken to be the particle number operators, for which $\lambda_{\max} = N$ and $\lambda_{\min} = 0$, we can write

$$\Delta G_{\mathrm{L}} = \frac{k}{2}N, \qquad \Delta G_{\mathrm{NL}} = \frac{1}{2}N^k, \quad (2.46)$$

whence

$$\Delta\phi_{\mathrm{L}} \geqslant \frac{1}{kN}, \qquad \Delta\phi_{\mathrm{NL}} \geqslant \frac{1}{N^k}. \quad (2.47)$$

We also note the following terminology, which has become established in quantum metrology. At $k = 1$, the Hamiltonian of the physical process corresponding to the evolution of the unknown (phase) parameter depends linearly on the number of particles, $\hat{H} \propto \phi\hat{N}$, and it is therefore appropriate to speak about *linear quantum metrology*. The maximum achievable accuracy of ϕ measurements is the HL $\Delta\phi \geqslant N^{-1}$.

The transformation generators $\hat{G}_{\mathrm{NL}}$ in (2.46) with $k > 1$ pertain to *nonlinear metrology* of some phase parameter involved in the process of nonlinear phase shift $\hat{H} \propto \phi\hat{N}^k$, and hence the expression

$$\Delta\phi \geqslant \frac{1}{N^k} \quad (2.48)$$

is a super-Heisenberg limit of the measurement (estimate) of the phase parameter. Expression (2.48) allows describing the ultimate accuracy in both linear ($k = 1$) and nonlinear ($k > 1$) quantum metrology in a unified way. For simplicity, in what follows, we speak of (2.48) as the generalized Heisenberg limit (GHL).

Thus, the maximum metrological accuracy (without taking losses into account) that can be achieved in view of (2.47) is in the range

$$\frac{1}{N^k} \leqslant \Delta\phi \leqslant \frac{1}{N^{k-1/2}}. \quad (2.49)$$

The right-hand side of (2.49) is a generalization of the SQL to nonlinear metrology and can be obtained using probe coherent states (2.49) under the same condition of a nonlinear phase shift $\hat{H} \propto \phi\hat{N}^k$ [79, 80]. Interestingly, the error $\Delta\phi$ of measuring the unknown parameter ϕ in nonlinear metrology overcomes the SQL $\Delta\phi = 1/\sqrt{N}$ by orders of magnitude of N, even if the interferometer input contains coherent states.

From a practical standpoint, an important limit case of (2.49) is the estimate of the unknown parameter of the cubic nonlinearity of the medium, for which $k = 2$ and which corresponds to the self-action of a plane (light) wave in such a medium. However, as was shown in [44, 81], quantum nonlinear metrology with (spatial) bright solitons leads to an estimate of the metrological window of quantum measurements of the Kerr nonlinearity parameter in the form

$$\frac{1}{N^3} \leqslant \Delta\phi \leqslant \frac{1}{N^{2.5}}, \quad (2.50)$$

which formally corresponds to the value $k = 3$ in (2.49). From a physical standpoint, this is because of spatial nonlinear effects that occur during the formation of bright solitons. A practically important contribution would be provided by the experimental confirmation of inequalities (2.50) based on optical or atomic bright solitons. However, for now, obtaining quantum regimes for such solitons with a relatively small (mesoscopic) number of particles faces objective challenges. In optics, with a small Kerr nonlinearity parameter, solitons typically contain a macroscopically large number of photons, $N \simeq 10^6$ [82] or more, and experience decoherence at a significant level for such problems. Some hopes are pinned on the use of semiconducting media with high cubic nonlinearity. In experiments with nonequilibrium exciton–polariton condensates, it was possible to obtain bright solitons with a mesoscopic number of particles (in the hundreds) [83]. However, such media are 'highly noisy' (at least at observation temperatures of several kelvins) due to the excitation of a large reservoir of excitons and the finite lifetime of photons in the microcavity [84].

In atomic optics, Bose–Einstein condensates, which have a negative scattering length, allow obtaining solitons with a mesoscopic number of atoms $N \simeq 10^3$ [85]. However, such experiments are still unique because bright solitons form in a fairly narrow range of the number of particles that satisfy the soliton stability condition.

Thus, expression (2.49) shows that the nonlinear metrology options for overcoming the SQL with an increasing parameter $k > 1$ significantly broaden. However, the use of purely nonlinear media forming the corresponding phase parameters is generally associated with an increase in noise, dissipation, thermal fluctuations, and so on. The use of quantum metrological schemes based on highly nonlinear media has be to physically justified in each particular case [86].

3. Limit measurements and detection of phase parameters in quantum optics

3.1 Quantum measurements with squeezed states of light

Historically, states with squeezed fluctuations of the electromagnetic field were among the first ones proposed for measuring small displacements beyond the SQL in an MI [6]. Today, there are numerous reviews devoted to squeezed and correlated states of the light field, and we note one among the most recent of them [87]. In studies dating back to the 1980s–1990s, the main emphasis was on various fundamental properties of nonclassical states of light and on measurements with them (see, e.g., [88–96]). Currently, such states are of great practical interest from the standpoint of various applications, in quantum metrology and sensing, as well as in quantum communications and quantum computing [74, 97–101]. Similarly to coherent states (2.33), they are states with continuous field variables, which can be characterized by some complex number $\zeta \equiv r\exp(\mathrm{i}\theta)$, where r and θ are the squeezing parameter and phase. The SMSV state in (2.38) can be realized in the general form by applying the squeezing operator $\hat{S}(\zeta) = \exp[(1/2)\zeta^* \hat{a}^2 - (1/2)\zeta \hat{a}^{\dagger 2}]$ to the vacuum state, i.e., as $|\mathrm{SMSV}\rangle = \hat{S}(\zeta)|0\rangle$.

Physically, the SMSV state can be obtained as a result of frequency-degenerate SPDC of light, when a pump field photon decays into two twin photons, identical in frequency (and polarization) (Fig. 3).

In a more general case where photons 1 and 2 differ at least in polarization, such a process is described by the squeezing operator $\hat{S}_{12}(\zeta) = \exp[\zeta^* \hat{a}_1 \hat{a}_2 - \zeta \hat{a}_1^\dagger \hat{a}_2^\dagger]$, which allows obtaining a two-mode squeezed vacuum (TMSV):

$$|\mathrm{TMSV}\rangle_{12} = \hat{S}_{12}(\zeta)|0\rangle_1|0\rangle_2 = \frac{1}{\cosh(r)} \sum_{n=0}^{\infty} (-1)^n \tanh^n(r) \exp(\mathrm{i}n\theta)|n\rangle_1|n\rangle_2 . \quad (3.1)$$

It readily follows from (2.38) and (3.1) that the corresponding light radiation states $|\mathrm{TMSV}\rangle_{12}$ (except the vacuum) at the exit from a nonlinear crystal always contain an even number of photons. These states have several remarkable statistical properties, which are well known and which allow using the states in various applications of modern quantum optical technologies [98]. For example, quantum properties of the SMSV state are due to the behavior of Hermitian quadratures of the light field, analogous to the coordinate $\hat{q}$ and momentum $\hat{p}$ in quantum mechanics (cf. (2.1)),

$$\hat{Q} = \frac{1}{2}(\hat{a}^\dagger + \hat{a}), \qquad \hat{P} = \frac{\mathrm{i}}{2}(\hat{a}^\dagger - \hat{a}). \quad (3.2)$$

The commutation relation $[\hat{Q}, \hat{P}] = \mathrm{i}/2$ between operators (3.2) leads to the Heisenberg uncertainty relation

$$\Delta Q^2 \Delta P^2 \geqslant \frac{1}{16}, \quad (3.3)$$

which makes a simultaneous exact measurement of the corresponding light field quadratures impossible. With the optimal value chosen for the squeezing phase θ, we can obtain the SMSV state dispersions in (3.3) as

$$\Delta Q^2 = \frac{1}{4}\exp(\mp 2r), \qquad \Delta P^2 = \frac{1}{4}\exp(\pm 2r), \quad (3.4)$$

which correspond to the squeezing phase $\theta = 0$ (the upper signs) and $\theta = \pi$ (the lower signs).

Expressions (3.4) demonstrate the effects of squeezing, which consists of an exponential decrease in one of the quadrature dispersions, and of antisqueezing, which is an increase in the dispersion of fluctuations in the phase-conjugate quadrature with increasing squeezing parameter r. The coefficient $1/4$ in (3.4) gives the value of the dispersion for the vacuum or coherent states of light at $r = 0$. This allows interpreting squeezed states as those with fluctuations suppressed below the shot noise level. We note that the uncertainty relation valid for the dispersions of quadratures in (3.3) takes a minimum value and is not violated for any θ or r.

The parameter r in (3.1) describes the SPDC efficiency and depends on the crystal thickness L, its quadratic nonlinearity $\chi^{(2)}$, and the classical pump wave amplitude $\sqrt{I_\mathrm{p}}$ (where I_p is the intensity), such that $r \propto \chi^{(2)}\sqrt{I_\mathrm{p}}L$ [101]. As follows from (3.1), ideal (100%) squeezing $\langle(\Delta\hat{Q})^2\rangle \to 0$ can be achieved only in the limit as $r \to \infty$, which physically requires infinitely large values of the above parameters. In experiments with squeezed light, a nonlinear crystal is placed in a cavity in order to effectively increase L (cf. [14]). In practice, the quadrature dispersions are always limited due to radiation losses and the finite value of r. The squeezing level is directly related to the squeezing parameter, which in turn is determined by the pump power of the nonlinear crystal. This level is usually measured in dB, calculated as

$$[\mathrm{dB}] = -10\log_{10}\left(\frac{\Delta X^2}{\Delta X^2_\mathrm{vac}}\right) = -10\log_{10}\left(\exp(-2r)\right), \quad (3.5)$$

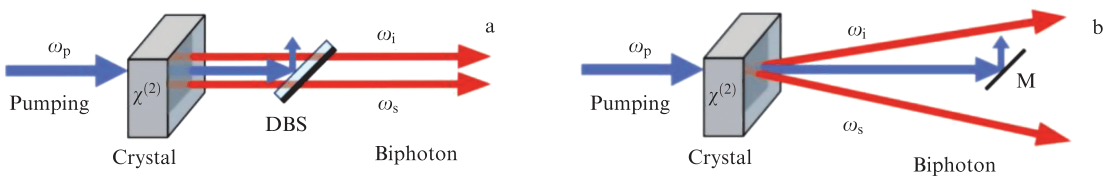

Figure 3. (a) Degenerate and (b) nondegenerate SPDC in a crystal with quadratic nonlinearity $\chi^{(2)}$, which allows obtaining respective single-mode (a) and two-mode (b) squeezed states. DBS is a dichroic beamsplitter, M is a mirror, and ω_p, ω_i, and ω_s are circular frequencies of pump, idler, and signal photons.

where $\hat{X} = \{\hat{Q}, \hat{P}\}_{\min}$ is the minimum of the two quadratures and $\Delta X^2_{\text{vac}} \equiv \langle(\Delta\hat{X})^2\rangle_{\text{vac}}$ is dispersion for the vacuum state. The last equality in (3.5) holds in view of (3.4). For example, for a 15-dB squeezing, as was obtained experimentally in [102], the formal squeezing parameter calculated in accordance with (3.5) is $r \simeq 1.73$.

Losses in squeezed-light setups can be estimated using the method of fictitious beamsplitters (see Section 5). The essence of the method is that (fictitious) beamsplitters are added to the setup to deflect some of the photons; this is equivalent to accounting for losses and/or interaction with the environment represented by quantum modes (oscillators) in the vacuum state.

As a result, the measured quadrature dispersion (without taking the efficiency of detectors into account) becomes (cf. [101])

$$\Delta X^2_{\text{means}} = \eta\,\Delta X^2 + \frac{1-\eta}{4}\,, \tag{3.6}$$

where $\hat{X} = \{\hat{Q}, \hat{P}\}$ and η is the setup transmittance of $(0 \leqslant \eta \leqslant 1)$. In the ideal case, $\Delta X^2_{\text{means}} = \Delta X^2$ at $\eta = 1$. We note that, with (3.6) taken into account, the minimum product of dispersions (3.3) is no longer attainable.

Over the past 20 years, experiments with squeezed light have seen significant progress, due to the new hardware components of both linear and nonlinear elements that allow integrated implementation on a chip (see, e.g., [103, 104]). Figure 4 shows a simplified setup of the experiment to generate SMSV states [105], consisting of four main blocks. A fiber laser generates the working SMSV wavelength, the one used in schemes for gravitational wave detection. Its coherent radiation (the $|\alpha\rangle_1$ state) is used as the field of a local (reference) oscillator in the balanced homodyne detector block when registering SMSV states. The second-harmonic generation (SHG) block allows pumping at a wavelength of 0.775 μm, which is then used in the SPDC block, where the $|\text{SMSV}\rangle_2$ state forms (see (2.38)). We note that both the SHG and SPDC units involve cavities with quadratic nonlinear periodically polarized potassium titanyl phosphate crystals (PPTPCs) placed inside. As a result, the main factors limiting the squeezing of one of the quadratures is the efficiency of radiation conversion in these media. To be specific, for theoretical estimates of the setup in Fig. 4, the phase-optimized dispersion ΔX^2 of one of the squeezed light quadratures can be expressed as

$$\Delta X^2 = 1 + \eta\,\frac{4\sqrt{P/P_{\text{thr}}}}{\left(1-\sqrt{P/P_{\text{thr}}}\right)^2 + 4\Omega^2}\,, \tag{3.7}$$

where $\eta \simeq 0.965$ is the parameter responsible for the efficiency of detectors and SPDC, $P_{\text{thr}} \simeq 221$ mW is the threshold power of parametric generation in a nonlinear crystal, P is the pump power, and Ω is the ratio of the frequency at which squeezed light is measured (ranging from units to tens of MHz) to the losses in the cavity with the SPDC crystal. As a result, a 12.3-dB squeezing was obtained.

We now discuss how squeezed states of light are used to improve the accuracy of measurements in optical interferometers (cf. [14, 18]). For this, we analyze the measurement accuracy in an MZI in the case where the initial state at the first MZI beamsplitter (Fig. 2b) is a combination of coherent light and an SMSV, $|\psi_{\text{in}}\rangle = |\alpha\rangle_1|\text{SMSV}\rangle_2$, which corresponds to quantum metrology with the CSV state, for which the

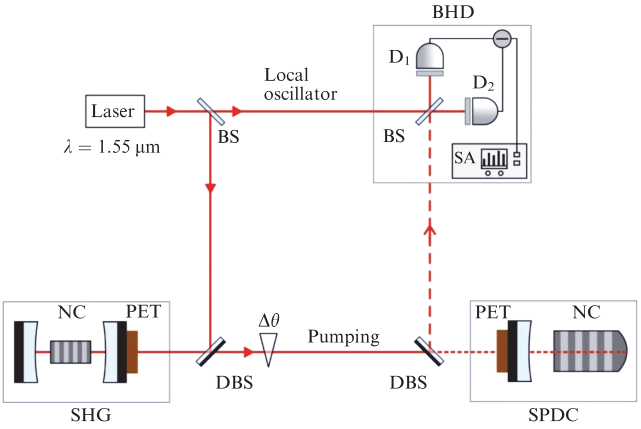

Figure 4. Simplified diagram of generating and detecting SMSV states [105]: SHG — second harmonic generation unit, SPDC — unit with spontaneous parametric down conversion, BHD — balanced homodyne detector, DBS — dichroic beamsplitter, BS — semitransparent beamsplitter, PET — piezoelectric element, SA — spectrum analyzer, NC — nonlinear crystal, $\Delta\theta$ — pump phase control element.

average number of photons is

$$\langle\hat{N}\rangle = |\alpha|^2 + \sinh^2(r)\,. \tag{3.8}$$

The first term in (3.8) corresponds to the coherent part of the field at the entrance to the MZI, and the second corresponds to the average number of noise photons generated in SPDC (the second term is the average number of photons in the SMSV state, as noted in Table 1). In this case, taking ζ to be real for simplicity and calculating similarly to what was done in (2.29)–(2.32) for a part of the interference pattern formed on the MZI detectors (at $\phi_0 = \pi/2$), we obtain the error shift of the phase parameter $\Delta\phi$ in the form (cf. [11, 52])

$$\Delta\phi = \frac{\sqrt{|\alpha|^2\exp(-2r) + \sinh^2(r)}}{\left||\alpha|^2 - \sinh^2(r)\right|}\,. \tag{3.9}$$

We assume that the coherent field component at the entrance to the MZI is much greater than the noise component, i.e., $N \simeq |\alpha|^2 \gg \sinh^2(r)$. From (3.9), we then have

$$\Delta\phi \simeq \frac{\exp(-r)}{\sqrt{N}}\,, \tag{3.10}$$

which means that it is in principle possible to overcome the SQL using SMSV states (cf. [6]). The dependence on r in (3.10) has been confirmed in experiment. Already in pioneering study [106] devoted to the use of squeezed states in metrology, a 2-dB quadrature suppression was achieved. The experiment was based on the same scheme involving an MZI, in which a quadratic nonlinear SPDC crystal was placed in one the arms to generate the SMSV states. To date, a record level of suppression of quadrature dispersion of light radiation was achieved in [102] with a quadratically nonlinear PPTPC crystal 9.3 mm in length. The squeezed light was detected with a 99.5% efficiency in a standard manner using balanced homodyne detection and calibrated InGaAs p–i–n photodiodes.

Importantly, expressions (3.9) and (3.10) are essentially the result of using formula (2.19), which characterizes the propagation of the phase measurement error in the SMSV experiments described above. Formula (2.19) does not answer the question as to what extent Eqns (3.9) and (3.10) correspond to the allowed limit measurements of the phase parameter, because it does reflect various strategies for measuring, detecting, and estimating the phase parameter. In this regard, a more precise approach would be to estimate the maximum measurement accuracy in the formalism of Fisher information (2.10), (2.11), which is unrelated to a specific measurement/detection scheme and allows estimating the maximum information gleaned when assessing an a priori unknown phase parameter. These issues were extensively discussed in [52, 53]. In particular, the use of (2.7) to calculate Fisher information allows estimating the phase error $\Delta\phi$ in a way that turns out to be independent of the phase ϕ itself,

$$\Delta\phi = \frac{1}{\sqrt{|\alpha|^2 \exp(2r) + \sinh^2(r)}}, \tag{3.11}$$

and hence the 'classical' (reference) phase ϕ_0 can take values in the range $0 \leqslant \phi_0 \leqslant \pi$. It follows from (3.11) that $\Delta\phi$ reaches the SQL at $|\alpha|^2 = 0$ and $\sinh^2(r) = N$, when the initial state is just the SMSV. Similarly, if initially we have only the coherent state with $N = |\alpha|^2$ ($r = 0$), then Eqn (3.11) implies SQL (2.35). The optimum situation from the metrology standpoint is the one where

$$|\alpha|^2 \simeq \sinh^2(r) \simeq \frac{\exp(2r)}{4} \simeq \frac{N}{2}. \tag{3.12}$$

In this case, estimating the phase parameter leads to the HL $\Delta\phi = 1/N$. Because the squeezing parameter r is small in practice, expression (3.8) imposes stringent restrictions on the amplitude of the coherent field α. For example, to obtain a noticeable squeezing of one of the quadratures at a 15-dB level, the squeezing parameter must be $r \simeq 1.73$ (cf. [107]), and the average number of photons in the coherent field $|\alpha|^2 \simeq 8$, which is much less than the values corresponding to the laser field intensities in gravitational wave detection schemes [6]. These limitations may be overcome (at least in theory) by using more complex unbalanced interferometers with SU(1, 1) symmetry, containing quadratic nonlinear crystals instead of beamsplitters (see [54]), but such schemes require careful experimental selection of phase parameters, the squeezing and antisqueezing parameters, losses, and so on.

In this review, we mainly consider SU(2) interferometers, which essentially allow high-precision measurements of unknown phase parameters with both macroscopic and small numbers of photons. Of interest in the last case, in view of the developing technologies for detecting quantum states of light (see, e.g., [31]), which we discuss in what follows, are entangled states with a fixed total number of photons, and $N00N$ states in particular.

3.2 Detecting quantum states with ultimate sensitivity

We study the physical criteria that must be satisfied by light radiation sources and detection setups to achieve the HL. Physically, the GHL in (2.48) can be achieved by using the so-called $N00N$ state, which is maximally entangled in path, at the entrance to the interferometer. As can be seen from (2.44), the $N00N$ state is a superposition of two Fock states: one describes N photons in channel 1 and none in channel 2, and the other, N photons in channel 2 and none in channel 1. The problem of obtaining and using state (2.44) in practice is discussed in more detail in subsequent sections. Here, we only address the detection of a quantum state at the exit from an MZI and analyze the interference pattern and estimate the phase ϕ. Namely, we assume that one single-photon detector is placed in arm 2 of the MZI (Fig. 2b) and that this detector can distinguish how many photons hit it simultaneously. It can then also measure the parity of the number of incident photons, i.e., the quantity described by the operator

$$\hat{\Pi}_2 = (-1)^{\hat{a}_2^\dagger \hat{a}_2} = \exp(\mathrm{i}\pi \hat{a}_2^\dagger \hat{a}_2) = \exp(\mathrm{i}\pi \hat{J}) \exp(-\mathrm{i}\pi \hat{J}_Z), \tag{3.13}$$

where $\hat{J} = \hat{N}/2$. In the MZI shown in Fig. 2b, the evolution of the state $|\psi_{\mathrm{in}}\rangle \equiv |N00N\rangle$ in (2.44) is described by the operator

$$\hat{U}_{\mathrm{MZ}} = \hat{U}_{\mathrm{BS}}^\dagger \hat{U}_\varphi = \exp\left(\mathrm{i}\frac{\pi}{2}\hat{J}_X\right) \exp(-\mathrm{i}\varphi \hat{J}_Z) \tag{3.14}$$

and (up to the overall phase) leads to

$$|\psi_{\mathrm{out}}\rangle = \hat{U}_{\mathrm{MZ}}|\psi_{\mathrm{in}}\rangle = \exp\left(\mathrm{i}\frac{\pi}{2}\hat{J}_X\right) \frac{|N,0\rangle + \exp(\mathrm{i}N\varphi)|0,N\rangle}{\sqrt{2}}, \tag{3.15}$$

where φ is the phase shift in the MZI, given the reference phase ϕ_0 and the information about the measured parameter ϕ. In the simplest case $\phi_0 = 0$, we have $\varphi = \phi$ (cf. (2.27) and (2.28)). Therefore, the average of operator (3.13) at the exit from the MZI can be described as

$$\langle \hat{\Pi}_2 \rangle = \langle \psi_{\mathrm{in}}| \hat{U}_{\mathrm{MZ}}^\dagger \hat{\Pi}_2 \hat{U}_{\mathrm{MZ}} |\psi_{\mathrm{in}}\rangle = \langle \psi_{\mathrm{in}}| \exp(\mathrm{i}\pi \hat{J}) \exp(\mathrm{i}\varphi \hat{J}_Z) \times \left[\exp\left(-\mathrm{i}\frac{\pi}{2}\hat{J}_X\right) \exp(-\mathrm{i}\pi \hat{J}_Z) \exp\left(\mathrm{i}\frac{\pi}{2}\hat{J}_X\right)\right] \exp(-\mathrm{i}\varphi \hat{J}_Z) |\psi_{\mathrm{in}}\rangle. \tag{3.16}$$

After simple calculations [72, 108], we obtain

$$\langle \hat{\Pi}_2 \rangle = \begin{cases} (-1)^{N/2} \cos(\varphi N), & \text{if } N \text{ is even}, \\ (-1)^{(N+1)/2} \sin(\varphi N), & \text{if } N \text{ is odd}. \end{cases} \tag{3.17}$$

Furthermore, because $\hat{\Pi}_2^2 \equiv \hat{\mathbf{I}}$ is the unit operator, which does not change the state it acts on, the dispersion of operator (3.13) averaged over state (2.44) is given by

$$\Delta\Pi_2^2 = \langle \hat{\Pi}_2^2 \rangle - \langle \hat{\Pi}_2 \rangle^2 = \begin{cases} \sin^2(\varphi N), & \text{if } N \text{ is even}, \\ \cos^2(\varphi N), & \text{if } N \text{ is odd}. \end{cases} \tag{3.18}$$

Expressions (3.17) and (3.18) have an important physical interpretation. Parity detectors can detect N-photon events, namely, the interference of N photons. From the error increase expression in (2.32), the error of measuring the phase parameter ϕ, on which the phase φ depends, follows in the form

$$\Delta\phi = \frac{\Delta\Pi_2}{\left|\partial\langle \hat{\Pi}_2 \rangle / \partial\phi\right|} = \frac{1}{N}\left|\frac{\partial\varphi}{\partial\phi}\right|^{-1}. \tag{3.19}$$

This implies that, using the MZI shown in Fig. 2b, the HL

$$\Delta\phi = \frac{1}{N} \tag{3.20}$$

is attained when measuring the small phase ϕ within the linear metrology framework, where $\varphi = \phi_0 + \phi$.

In nonlinear metrology problems, when a medium with an unknown Kerr nonlinearity is placed in an MZI arm, the phase φ should be assumed to depend on the number of photons N, $\varphi = N^{k-1}(\phi_0 + \phi)$, and the super-HL,

$$\Delta\phi = \frac{1}{N^k}\,, \tag{3.21}$$

then follows from (3.19) (cf. (2.48) and (2.47)).

Thus, it is the parity detector that in our case allows achieving the maximum metrological accuracy with the initial (probe) $N00N$ state.

Parity measurements currently represent an important avenue in the practical development of quantum optics and quantum information [109]. In a more general case, they are based on a detector that must be 'calibrated' to measure Fock states, i.e., to distinguish the incident photons. Currently, the most popular detectors are those whose operating principle is based on superconductivity [110]. Obvious progress in this direction over the past 10 years is already visible from a comparative analysis of studies [111–117]. The main advantage of the detectors under consideration is their high quantum efficiency (over 98%) in a wide spectral range, speed (ability to repeat measurements) at the level of nanoseconds or less, a low level of dark noise [118], and options to increase the number of measured photons. For example, the correlation function $g^{(N)}$ with $N = 15$ was recently measured experimentally in [111]. A disadvantage of such detectors is still the need to maintain ultra-low temperatures (down to 100 mK), and a decrease in the detection efficiency as the number of photons N increases. In addition, we mention the high cost of such devices compared to their semiconducting counterparts. It is obvious that, with the progress in quantum technologies in general, superconducting detectors will become quite accessible for applications in integrated photonics dealing with a mesoscopic number of photons (tens of particles). In this regard, special hopes can be pinned on new (superconducting) materials that demonstrate high sensitivity at moderately low temperatures (up to 25 K) [119].

3.3 Limit capabilities of quantum sensing

Expressions (3.17) and (3.18) show that an interference pattern can be observed with a period N times less than with one photon, which means superresolution of the phase ϕ (at $\phi_0 = 0$), i.e., its hypersensitivity [120, 121]. This interference pattern can be amplified by N^k times in the general case of nonlinear metrology.

In reality, however, the interference pattern has a finite visibility V ranging within $0 \leqslant V \leqslant 1$, and a measurement efficiency $0 \leqslant \eta \leqslant 1$. The probability of N-photon interference (within linear metrology) for one measurement with these quantities taken into account is

$$p = \frac{\eta}{2}\big(1 + V\sin(\varphi N)\big) \tag{3.22}$$

(cf. (3.17) and also [122]).

The phase estimate is then determined by the average rate of N-photon events in ν trials, i.e.,

$$C_\nu = \nu p\,. \tag{3.23}$$

In experiments, the number of trials ν is always finite, and hence C_ν has the standard deviation

$$\Delta C_\nu = \sqrt{\nu p(1-p)}\,. \tag{3.24}$$

Quantity (3.24) can be associated with the phase hypersensitivity S determined in the course of detecting the interference of N photons in the form

$$S = \frac{1}{\sqrt{\nu N}\,\Delta\phi}\,, \tag{3.25}$$

where $\Delta\phi$ is the measurement error of the phase ϕ, which can be expressed in terms of ΔC_ν using phase error propagation as

$$\Delta\phi = \frac{\Delta C_\nu}{|\partial C_\nu/\partial\phi|}\,. \tag{3.26}$$

Expression (3.25) can be interpreted differently if we use the definition of QCRB (2.8). We then estimate the parameter S in a measurement as

$$0 \leqslant S \leqslant \sqrt{\frac{F_q}{N}}\,, \tag{3.27}$$

where F_q is the QFI associated with the accuracy of measuring ϕ. Using (2.48), we arrive at the upper bound $S_{\max}$ for the phase measurement sensitivity in the form

$$S_{\max} = N^{k-1/2}\,. \tag{3.28}$$

On the other hand, under classical measurement conditions, it follows from (3.27) that

$$0 \leqslant S_{\mathrm{cl}} \leqslant 1\,, \tag{3.29}$$

where $S_{\mathrm{cl}} = 1$ corresponds to the SQL phase measurement with totally coherent light. Therefore, the quantum sensitivity of a sensor whose operation is based on the accuracy of measuring the phase parameter ϕ corresponds to the range

$$1 < S_q \leqslant N^{k-1/2}\,, \tag{3.30}$$

where $k = 1, 2, \ldots$.

In the case of a nonideal interference pattern considered above, described by the N-photon detection probability (3.22), the parameter S is given by [122]

$$S = \frac{\sqrt{0.5\eta N}V\big|\cos(\phi_0 N)\big|}{\sqrt{\big(1 + V\sin(\phi_0 N)\big)\big(1 - 0.5\eta\big(1 + V\sin(\phi_0 N)\big)\big)}}\,. \tag{3.31}$$

We see from (3.30) that S reaches its maximum value at the phase ϕ_0 satisfying the condition $|\cos(\phi_0 N)| = 1$, with

$$S = \frac{\sqrt{0.5\eta N}V}{\sqrt{1 - 0.5\eta}}\,. \tag{3.32}$$

We see that (3.32) depends on the interference pattern visibility V and the measurement efficiency η. In the limit of ideal visibility and detection $V, \eta \to 1$, we have $S \to \sqrt{N}$, which corresponds to the HL sensitivity of phase estimate (3.28) at $k = 1$.

4. Quantum metrology based on maximally entangled photon states

4.1 Hong–Ou–Mandel effect

A practically important resource of optical quantum metrology, allowing measurements at the HL level, is the $N00N$ state

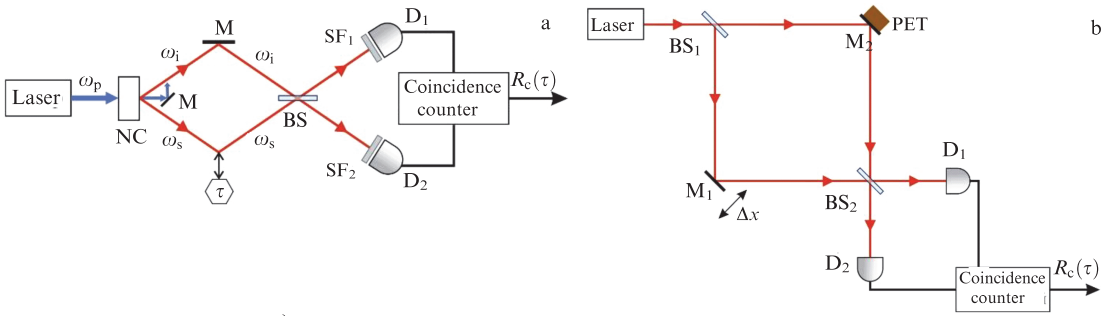

Figure 5. Schematics of (a) HOM experiment and (b) its analogue with weak coherent light pulses [127]: NC — quadratic nonlinear crystal of barium beta borate; ω_p, ω_s, and ω_i — frequencies of pump, signal, and idler photons; M — mirrors, BS — beamsplitter, $SF_{1,2}$ — spectral filters, $D_{1,2}$ — detectors, τ — time difference between signal and idle photons, $\Delta x = c\tau$ — optical path difference of photons (c is speed of light in vacuum), $R_c(\tau)$ — sought function of the number of detector coincidences during observation time; PET — piezoelectric element.

containing $N = 2$ photons (see (2.44)). The preparation of such states is based on the Hong–Ou–Mandel (HOM) interferometer (Fig. 5a); it allows identifying the HOM effect, manifesting one of the fundamental and practically most significant quantum effects associated with (destructive) quantum interference of photons on a beamsplitter [55].

The experiment to observe the HOM effect is based on SPDC in a nonlinear crystal, i.e., the decay of a pump laser photon with a frequency ω_p into two photons (so-called biphotons): the signal photon with a frequency ω_s and the idle photon with a frequency ω_i. In the general case, these frequencies have a distribution different from the delta function: in the stationary case, the frequencies are related to each other as $\bar{\omega}_s + \bar{\omega}_i = \omega_p$. The photons are then sent into two arms of the interferometer (see Fig. 5a and [123]).

The biphoton travel time difference τ can be caused by various physical processes: elongation of an optical fiber placed in a heated/cooled environment, shift of installation elements, and so on. Hence, if we take the travel time of the idler photon as a reference, then only a change in the travel time τ of the signal photon is considered. The dispersion of the medium in which the biphoton field propagates also leads to a temporal shift τ. Finally, the interferometric setup itself can introduce some displacement and the resultant delay τ_0. After mixing the signal and idler photons on a beamsplitter, the photons are recorded by detectors in the coincidence counting regime. In other words, the probability $R_c(\tau)$ is recorded for two photons to arrive at two detectors simultaneously, i.e., the quantum state $|1,1\rangle$. The minimum of $R_c(\tau)$, known as the HOM dip in the literature, is formed at $\tau = 0$ and is associated just with the HOM effect [124]. The shape of the anti-correlation dip corresponds to the inverted envelope, squeezed by a factor of two, of the correlation function $g^{(1)}(\tau)$ of the first order in intensity (of the second order in the field) [125],

$$R_c \sim 1 - g^{(1)}(2\tau)\,, \tag{4.1}$$

which is related to the spectral density of the field by the Wiener–Khinchin theorem [126].

In the case — important from an experimental standpoint — where narrow-band filters are installed in front of detectors with the spectral transmission described by a Gaussian function with a width σ_p,[2] the shape of the dip is determined by this Gaussian, but is still $\sqrt{2}$ times narrower than the corresponding correlation function $g^{(1)}(\tau)$:

$$R_c \sim 1 - \frac{1}{2\pi}\int \exp\left(-\frac{\Omega^2}{4\sigma_p^2}\right)\cos(\Omega\tau)\,\mathrm{d}\Omega\,. \tag{4.2}$$

Here, $\Omega = \omega - \omega_0$ is the frequency detuning from the central frequency ω_0 of the SPDC spectrum in the degenerate regime ($2\omega_0 = \omega_p$).

To understand what causes the dip and to estimate its magnitude in experiment, it is useful to consider a simple physical picture with two photons that are prepared using a nonlinear crystal and are incident on a semitransparent beamsplitter, as shown in Fig. 5a. The initial state at the entrance to the beamsplitter is

$$|\psi_{in}\rangle = |1,1\rangle = \hat{a}_1^\dagger \hat{a}_2^\dagger |0\rangle\,. \tag{4.3}$$

The state at the exit from the beamsplitter depends on the distinguishability and statistics [55]. For $\tau = 0$, in the general case, we can write

$$|\psi_{out}\rangle = \frac{1}{2}\left((\hat{a}_1^\dagger)^2 - (\hat{a}_2^\dagger)^2\right)|0\rangle + \frac{1}{2}(\hat{a}_2^\dagger \hat{a}_1^\dagger - \hat{a}_1^\dagger \hat{a}_2^\dagger)|0\rangle\,. \tag{4.4}$$

Expression (4.4) is sufficiently universal: it describes the experiment on the passage of particles through a beamsplitter not only for photons, which are bosons and which we discuss here, but also for fermions [55]. Due to the indistinguishability of bosons, the last term in (4.4) vanishes. Then, the probabilities of detecting one photon on each of the detectors, $P(1,1) = |\langle 1,1|\psi_{out}\rangle|^2$, and two photons on any of the detectors, $P(2,0) = P(0,2) = |\langle 2,0|\psi_{out}\rangle|^2$, are given by

$$P_{11} \equiv P(1,1) = 0\,, \qquad P_{20} \equiv P(2,0) = P(0,2) = \frac{1}{2}\,. \tag{4.5}$$

We see from Table 2 that subtraction of the corresponding probability amplitudes leads to destructive interference on the beamsplitter, which gives rise to the HOM dip (Fig. 6). In addition, because $(\hat{a}_i^\dagger)^2|0\rangle = \sqrt{2}|2\rangle$, the state of photons at the exit from the beamsplitter, up to an overall factor, can be written as

$$|\psi_{out}\rangle = \frac{1}{\sqrt{2}}\left(|2,0\rangle - |0,2\rangle\right), \tag{4.6}$$

which, up to a sign of the second term (the phase factor $\exp(i\pi) = -1$), coincides with the $N00N$ state (2.44) for $N = 2$. Thus, by analyzing the entire setup in Fig. 5a, we can

[2] This refers to the case where the filter spectrum is narrower than the SPDC spectrum.

Table 2. Elementary physical processes of transformation (transmission/reflection) of two photons in a semitransparent beamsplitter, contributing to individual probabilities of their detection at beamsplitter exit in quantum and classical cases. Second column (P_{11}) shows probabilities of events of simultaneous registration of one photon at BS exit; third column ($P_{20/02}$) corresponds to the case of transmission and reflection of both photons.

Particles	Photon registration probabilities	
	P_{11}	$P_{20/02}$
Quantum (bosons), indistinguishable	$\left\vert\ \ -\ \ \right\vert^2$	$\left\vert\ \ \right\vert^2, \left\vert\ \ \right\vert^2$
Classical, completely distinguishable	$\left\vert\ \ \right\vert^2, \left\vert\ \ \right\vert^2$	$\left\vert\ \ \right\vert^2, \left\vert\ \ \right\vert^2$

say that, in the ideal (quantum) case, the SPDC process in a BBO crystal generates two identical photons with frequencies $\omega_s = \omega_i = \omega_p/2$, which at $\tau = 0$ simultaneously hit the beamsplitter, which, due to interference, gives rise to the two-photon $N00N$ state (4.6) at its exit; in the case of ideal operation of the detectors, this ensures the maximum dip of the function $R_c(0) = 0$ (red curve in Fig. 6a).

4.2. Impact of classical noise on Hong–Ou–Mandel effect and photon indistinguishability

In a real experiment, due to inevitable classical noise, it is impossible to prepare two identical photons with 100% fidelity; only the equality of the average frequencies $\bar{\omega}_s = \bar{\omega}_i = \omega_p/2$ and fulfillment of the energy conservation law $\omega_s + \omega_i = \omega_p$ can be guaranteed in a series of such experiments. As a result of the nonidentity of the signal and idler photons, interference on the beamsplitter is violated and the dip loses its depth $R_c(0) > 0$; in experiments, this corresponds to a decrease in the visibility of the interference pattern.

In experiments, therefore, particles can be partially or even completely distinguishable by their frequency, polarization, and so on. To take this factor into account, photons should be regarded as single-particle wave packets

$$|\psi_{in}\rangle = \iint d\omega_s\, d\omega_i\, f(\omega_s, \omega_i)\, \hat{a}_1^\dagger(\omega_s)\hat{a}_2^\dagger(\omega_i)|0\rangle\,, \tag{4.7}$$

where $\hat{a}_1^\dagger(\omega_s)$ is the operator of the creation of the signal photon in arm 1 with the frequency ω_s and $\hat{a}_2^\dagger(\omega_i)$ is a similar operator for the idler photon in arm 2, with

$$\left[\hat{a}_k^\dagger(\omega_1), \hat{a}_l(\omega_2)\right] = \delta_{kl}\delta(\omega_1 - \omega_2)\,. \tag{4.8}$$

In (4.7), $f(\omega_s, \omega_i)$ is the joint spectral intensity (JSI) function, which in the most general form can be written as

$$f(\omega_s, \omega_i) = C f_s(\omega_s + \omega_i) f_{pm}(\omega_s, \omega_i)\,, \tag{4.9}$$

where C is the normalization constant, $f_s(\omega_s + \omega_i)$ is the pump spectrum profile, and $f_{pm}(\omega_s, \omega_i)$ is the phase-matching function:

$$f_{pm}(\omega_s, \omega_i) = \operatorname{sinc}\left(\frac{L}{2}\left(k_p(\omega_s + \omega_i) - k_s(\omega_s) - k_i(\omega_i)\right)\right) \times \exp\left(-i\,\frac{L}{2}\left(k_p(\omega_p) - k_s(\omega_s) - k_i(\omega_i)\right)\right). \tag{4.10}$$

Here, $k_p(\omega_p)$ is the dispersion of the pump wavenumber, and, similarly, $k_s(\omega_s)$ and $k_i(\omega_i)$ are dispersions for the signal and idler photons; L is the crystal thickness.

If the pump is narrowband (with a spectral linewidth $\sigma_p \ll 10$ THz or, in terms of the wavelength, $\Delta\lambda \ll 1$ nm), the JSI function coincides in absolute value with a Gaussian pump profile:

$$f(\omega_s, \omega_i) = \exp\left(-\frac{1}{2}\left(\frac{(\omega_s - \bar{\omega}_s) + (\omega_i - \bar{\omega}_i)}{\sigma_p}\right)^2\right) \times \exp\left(-i\,\frac{L}{2}\left(\frac{1}{v_p} - \frac{1}{v_s}\right)(\omega_s - \bar{\omega}_s) - i\,\frac{L}{2}\left(\frac{1}{v_p} - \frac{1}{v_i}\right)(\omega_i - \bar{\omega}_i)\right). \tag{4.11}$$

The phase factor in (4.11) arises due to the differences among group velocities of the pump, idler, and signal photons v_p, v_i, and v_s [128, 129]. In general, the criterion for a narrowband pump is the condition $\sigma_p \ll v_j/L$, where L is the thickness of the optical crystal and $j = p, i, s$.

From a physical standpoint, the loss of quantum indistinguishability of particles has a negative impact of classical noise on the visibility of the interference pattern. This effect can be taken into account if we assume that an additional

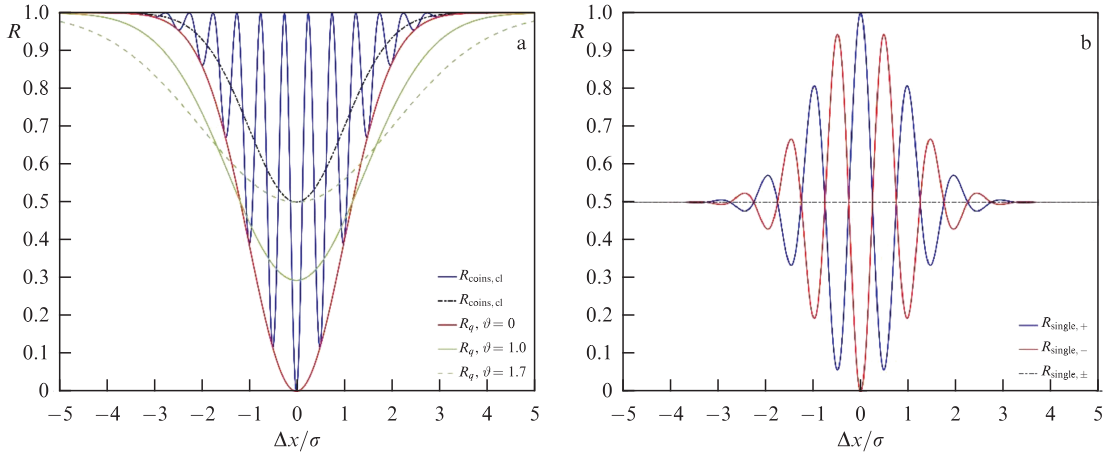

Figure 6. Quantum interference of single photons in HOM experiment and its 'classical' analogue with weak coherent light pulses. Probability of (a) joint and (b) single activation of detectors (see Fig. 5). Red solid and green lines in (a) are obtained from quantum (bosonic) probabilities with classical noise taken into account (see (4.13)). Black dashed-dotted lines correspond to classical metrology limit with averaging of rapidly oscillating components for $\sigma \gg \lambda_0$ (where σ is width of HOM dip at height $e^{-1/2}$). Oscillating curves in (b) (see expression (4.16)) and blue curve in (a) (see expression (4.17)) are due to interference for state (4.15); $\sigma = 1000\lambda_0$.

random phase shift $\exp(\mathrm{i}\epsilon\omega_s)$ occurs between photons, assigned, for example, to the signal photon. Here, ϵ is a classical random (fluctuating) quantity with a Gaussian distribution

$$g(\epsilon) = \frac{1}{\sqrt{2\pi}\sigma_\epsilon} \exp\left(-\frac{\epsilon^2}{2\sigma_\epsilon^2}\right). \tag{4.12}$$

After simple calculations with the JSI function, we obtain (cf. [130])

$$R_q(\tau) = 1 - \frac{1}{\sqrt{1+\vartheta^2}} \exp\left(-\frac{1}{1+\vartheta^2}\frac{\Delta x^2}{2\sigma^2}\right), \tag{4.13}$$

where $\Delta x \equiv c(\tau - \tau_0)$, τ_0 determines the position of the minimum, σ is the HOM dip width in the ideal case without noise, determined by the width of the pump *spectrum* and the nonlinear BBO properties, and $\vartheta \equiv \sigma_\epsilon/\sigma \geqslant 0$ is the relative 'amount' of noise (the case $\vartheta = 0$ corresponds to the absence of noise). Figure 6a shows the corresponding dependences (4.13) for $\vartheta = 0$ (red solid curve), $\vartheta = 1$ (green solid curve), and $\vartheta = 1.7$ (green dotted curve). It can be seen that the presence of classical noise ($\vartheta \neq 0$) reduces the depth of the dip by a factor of $\sqrt{1+\vartheta^2}$ and increases its width proportionally.

An interesting experiment from the standpoint of metrology was performed in [131]. Based on the estimation of the Fisher information and the use of the maximum likelihood method, the measurement of an optical delay of 4.97 nm was demonstrated with an accuracy of 0.89, determined by the CRB. The spectral width of the biphoton field was about 160 nm (a PPTPC crystal, type I synchronism).

4.3 Classic limit of Hong–Ou–Mandel effect

To fully understand the behavior of the HOM dip, we consider the same experiment with photons at the entrance to a beamsplitter, assuming them to be completely classical (distinguishable) particles. These issues were discussed previously in [132] at different levels, including metaphysical ones. Some recent indications of progress in this field are related to the use of the HOM effect in boson sampling schemes (see, e.g., [132]).

For clarity, we imagine that both photons in Fig. 5b are classical particles simultaneously incident from different directions on a beamsplitter, which with some *classical* probability reflects or transmits these particles individually. In this case, if the beamsplitter is ideally semitransparent, then *four* equally probable outcomes of such an experiment are possible: each photon is reflected, each photon passes through, two photons are reflected, and two photons pass through. As a result, we have the classical probabilities (cf. (4.5))

$$P_{11} = \frac{1}{2}, \qquad P_{20} = \frac{1}{4}. \tag{4.14}$$

As can be seen from (4.14) and Table 2, the probability P_{11} of an event in which one photon (no matter which one) hits each of the detectors is the sum of the probabilities of their passage and reflection separately, and it is greater than the probabilities of the detection of two-photon events P_{20}. Thus, the complete indistinguishability of quantum particles, which allows operating with the amplitudes of quantum probabilities rather than with the probabilities themselves, leads to a dip in the visibility of the interference pattern in Fig. 6a. Partial visibility corresponds to the solid green curve in the figure.

An elegant experiment was recently described in [127], with the photons emitted by weak coherent pulses of light and prepared in a state corresponding to classical probabilities (4.14) (Fig. 5b). We assume that coherent radiation in a state $|\psi_{\text{in}}\rangle = |\alpha\rangle_1$ is delivered to the entrance to the interferometer, then at the beamsplitter BS_1 (used instead of the SPDC in the original HOM scheme (Fig. 5a)) it is split into two coherent beams in states $|\alpha\rangle_1$ and $|\alpha\rangle_2$ (Fig. 5b). If the incoming coherent beam is sufficiently weak and contains only two photons on average ($N = |\alpha|^2 = 2$), this scheme can be considered a specific ('classical') counterpart of the HOM experiment. Two-photon states of two types then form at the exit from BS_1. The first type is when both photons are in one arm of the interferometer, which corresponds to the two-photon $N00N$ state (4.6). The second type is when the two photons are in different arms, which corresponds to the $|1,1\rangle$ state. Therefore, the states at the exit from BS_1 can be written as

$$|\psi_{\text{out}}\rangle = \frac{1}{2}\left(|2,0\rangle - \exp(\mathrm{i}2\phi)\,|0,2\rangle\right) + \frac{1}{\sqrt{2}}|1,1\rangle, \tag{4.15}$$

where $\phi = 2\pi\Delta x/\lambda_0$ is the relative phase shift in the arms of the interferometer, depending on the optical path difference of the beams Δx, and λ_0 is the central wavelength of pump radiation. The factor of 2 occurs in (4.15) because $N = 2$ (Fig. 5b). It can be clearly seen from (4.15) that the reduction of the state $|\psi_{\text{out}}\rangle$ to any of the states $|1,1\rangle$, $|2,0\rangle$, or $|0,2\rangle$ leads to results similar to classical probabilities (4.14). But, this does not make the diagram in Fig. 5b entirely classical: state (4.15) is still quantum. Indeed, after mixing at BS_2, the beams reach detectors operating in the single-shot counting mode (when only one of the two detectors is triggered) or in the coincidence counting regime (when both detectors are triggered simultaneously). In the first case, the number of detector activations during the exposure time can be estimated as [127]

$$R_{\text{single},\pm}(\Delta x) \propto \frac{1}{2}\left[1 \pm \cos(\phi)\exp\left(-\frac{1}{2}\frac{\Delta x^2}{\sigma^2}\right)\right], \tag{4.16}$$

and, in the second, as

$$R_{\text{coins,cl}}(\Delta x) \propto 1 - \frac{1}{2}\left(1 + \cos(2\phi)\right)\exp\left(-\frac{1}{2}\frac{\Delta x^2}{\sigma^2}\right), \tag{4.17}$$

where σ is determined by the width of the Gaussian profile of the input coherent beam $|\alpha\rangle_1$.

As can be seen from (4.16), interferometry based on low-intensity laser beams leads to quantum interference of weak coherent light pulses (oscillations in Fig. 6b), reproducing the HOM effect with a dip in the form of an inverted Gaussian whose width is determined by the width of the initial wave packet (see Section 4.1).

The fully classical limit of (4.16), (4.17) corresponds to the disappearance of the interference pattern and can be obtained from (4.16), (4.17) by averaging the cosine function over fast spatial oscillations, leading to the expressions

$$\bar{R}_{\text{single},\pm}(\Delta x) \propto \frac{1}{2}, \qquad \bar{R}_{\text{coins,cl}}(\Delta x) \propto 1 - \frac{1}{2}\exp\left(-\frac{1}{2}\frac{\Delta x^2}{\sigma^2}\right). \tag{4.18}$$

Formulas (4.18) are illustrated in Fig. 6 with black (dashed-dotted) lines. Figure 6a, interestingly, shows a

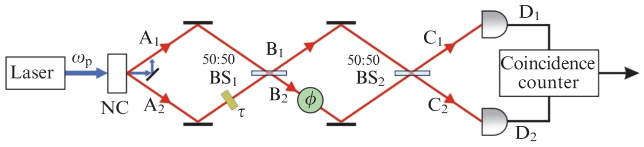

Figure 7. Quantum metrology schematic for unknown phase parameter ϕ, based on an HOM interferometer that receives biphotons (beams A_1 and A_2) as input and prepares state (4.7) (beams B_1 and B_2), combined with an MZI that completes preparation of final state (beams C_1 and C_2).

difference between the behavior of the probabilities of joint activation of detectors in the HOM setup under the effect of classical noise (green dashed curve at $\vartheta = 1.7$) and the limit (classical) averaged dependence $\bar{R}_{\text{coins, cl}}$ in (4.18); in both cases, the maximum value of the dip is the same, $R = 1/2$. Thus, this approach allows distinguishing the quantum HOM effect from its classical counterpart even in the presence of classical noise.

4.4 Quantum sensing with $N00N$ states and the problem of their preparation for $N > 2$

The $N00N$ states currently occupy a special place in quantum optical metrology, because they allow attaining the HL on any two-mode device: an interferometer, a gyroscope, a lithograph, etc.

Figure 7 shows a setup for measuring and estimating the phase ϕ using the $N00N$ state with $N = 2$. It is essentially a combination of a HOM interferometer with an MZI: state (4.6) is prepared at the output of the first beamsplitter and is then used in measuring ϕ (cf. [133]).

In experimental work [134], a setup similar to that shown in Fig. 7 was used to measure the concentration of bovine serum albumin (BSA) in an aqueous solution, a sample of which was placed in one of the MZI arms (green circle in Fig. 7). In addition, measurements were first carried out with distilled water to assess the level of losses and to determine the value of the reference phase $\phi_0 = \pi/2$. When a photon passed through the interferometer arm containing a BSA sample, the change in the refractive index Δn_s was found to depend linearly on the unknown phase ϕ,

$$\Delta n_s = \frac{\lambda}{2\pi L}\,\phi\,, \tag{4.19}$$

where $\lambda = 0.785$ μm and $L = 0.55$ μm is the wavelength and also the size of the microchannel with a BSA sample. In (4.19), the phase shift $\phi \propto C_s$ depends linearly on the BSA concentration C_s. The authors of [134] obtained the slope $\mathrm{d}n_s/\mathrm{d}C_s = (1.79 \pm 0.04) \times 10^{-3}$, which is consistent with the result $\mathrm{d}n_s/\mathrm{d}C_s = 1.82 \times 10^{-3}$ obtained at the wavelength $\lambda = 0.578$ μm by other methods [135].

In the course of measurements in [134], all combinations of the states $|2,0\rangle$, $|0,2\rangle$, and $|1,1\rangle$ were detected, which allowed comparing the visibility of interference patterns and estimating the loss level. It was found that the losses in the interferometer arms are asymmetric, leading to a limited measured visibility of the two-photon interference pattern, $V \simeq 82\%$. The obtained value turned out to be higher than the visibility $V \simeq 70.7\%$ corresponding to measurements at the SQL level, calculated for this experimental design in accordance with the method described in Section 2.4. The relatively small gain in measurement accuracy associated with V was attributed by the authors of [134] to the imperfection of the photodetectors.

It was shown in [136] that a temperature sensor can be built using the technique described here, based on the HOM effect. The MZI arm containing a section of quartz fiber was immersed in a temperature-controlled furnace. Even with a slight change in temperature, the fiber cladding thermally expanded, thereby changing the refractive index. The result of the measurements was $\mathrm{d}L/\mathrm{d}T \simeq 4.8 \times 10^{-7}$ m deg^{-1} with an accuracy of 0.12 deg (where L is the fiber length), which was also consistent with previously obtained data [137].

We note that, in addition to the effects of losses, the nonideal efficiency of detectors, and so on, the fundamental limitations of the methods under consideration are associated with the use of $N00N$ states with $N = 2$ photons. In this regard, an urgent and not fully studied task of modern quantum technologies in general is to obtain $N00N$ states with $N \geqslant 2$ that would be robust to losses. More precisely, we are talking about states that are not strictly $N00N$ states but are a superposition of entangled Fock states (cf. [138]). The preparation of such states is based, to one degree or another, on nonlinear elements of SPDC of light and also on linear optical elements: beamsplitters, phase plates, polarizers, analyzers, and so on (see, e.g., [60, 139]). Recently, the preparation of states with the desired quantum properties has become possible based on machine learning methods [140, 141]. It is noteworthy that, as the main basic elements for such states, the machine agent suggested actively using the solutions that had been proposed in [142].

It is important to keep in mind that the limited capabilities of modern detectors in measuring Fock states with a large number of photons and the fragility of $N00N$ states in measurements motivate attempts to solve the problem of quantum technologies outlined here using modern methods of integrated optics [143, 144]. Today, it is already possible to create waveguides and linear optics elements with ultra-low losses down to 0.1 dB cm^{-1} [145] and efficient parametric generators of entangled photon pairs [146]. Here, we focus on the method, in wide use recently, for obtaining $N00N$ states with continuous variables of light. From a physical standpoint, these are hybrid methods of information processing within a single optical setup, allowing one to obtain hybrid states of the light field by combining discrete and continuous field variables (see, e.g., [147]). The main problem in such setups is the need to eliminate 'superfluous' states present in the superposition along with the $N00N$ components. This can be done by preparing a conditioned state (a partial reduction of a quantum state) and/or postselection when processing the measurement results.

In [148], it was theoretically predicted for the first time that interference between coherent laser radiation and SPDC radiation gives rise to large-N $N00N$ states with a fidelity exceeding 90%. This method was experimentally implemented in the design of an ultrasensitive MZI-based microscope [149]. It involves the mixing of a coherent state with the SMSV at the first MZI beamsplitter (Fig. 8), which gives rise to the state (cf. [150])

$$|\psi_{\text{BS, out}}\rangle = \sum_{m=0}^{N} A_m |N-m, m\rangle\,, \tag{4.20}$$

at its exit; here, $|N-m,m\rangle \equiv |N-m\rangle_1 |m\rangle_2$ is the Fock state with a known number of photons N distributed over two modes with the probability coefficients A_m satisfying the

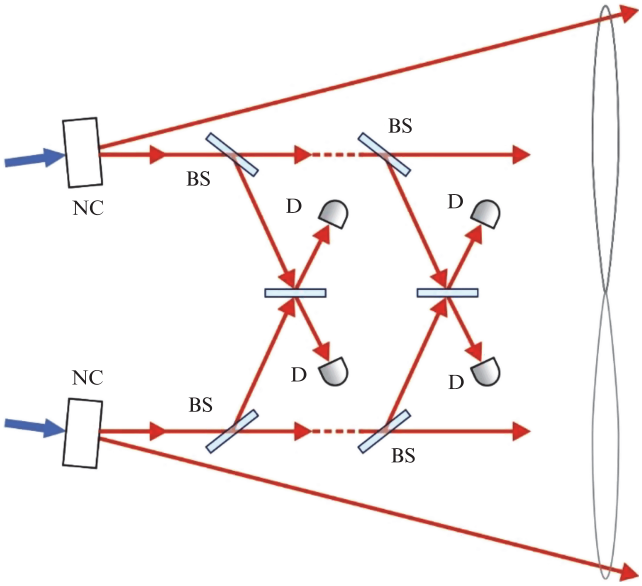

Fig. 8. Schematic for the preparation of a remote $N00N$ state: NC — nonlinear crystal, BS — semitransparent beamsplitter, D — detector. Blue arrows show pumping of crystals.

normalization condition $\sum_{m=0}^{N}|A_m|^2=1$. The interference pattern obtained in [151], recorded by measuring the coincidence probabilities for $N-m$ photons on one detector and m photons on the other, indicates that the 'superfluous' states can be eliminated from the sum in (4.20), i.e., we can have $A_1=A_2=\ldots=A_{N-1}=0$. An important point is to 'tune' the key parameters of the system: the phase $\theta_c\simeq\pi/2$ of the coherent state $\alpha=|\alpha|\exp(\mathrm{i}\theta_c)$ and the combination of parameters $\xi=|\alpha|^2/r$, where r is the squeezing parameter. In [151], the interference pattern was observed up to $N=5$, which corresponds to $\xi\simeq 2.16$. A further increase in N in [151] was limited by losses, inefficiency of detectors, etc., which the authors estimated with the help of an effective transmittance η for the entire setup: the value of η turned out to be about $\eta\simeq 0.12$ at $N=5$.

We note that a more complex setup based on the conditional (measurement-induced) preparation of $N00N$ states using the HOM effect was proposed in [152] (cf. [76]). In [150], the authors were the first to implement a method for remote preparation of $N00N$ states. Namely, the proposal was to use two identical TMSV sources, the output of which was a four-mode quantum state of pairwise entangled photons. One mode from each TMSV source was then sent through a quantum channel with a transmittance η to a block consisting of a sequence of $N/2$ beamsplitters, at the output of which photons were detected, leading to a partial reduction of the initial state to $N00N$ states of the remaining two modes with an even number of photons (the cases $N=2$, 4, and 6 were analyzed in the cited paper). For a small squeezing parameter $r\ll 1$, it was shown in [150] that the fidelity of preparing $N00N$ states is

$$F_I\simeq 1-(N+2)r^2\,, \tag{4.21}$$

which, for relatively small N, allows obtaining $N00N$ states with high fidelity. A minor challenge of the proposed method is a small total amplitude of $N00N$ states (before the normalization), which decreases as r^N, which determines the optimal probability of preparing such a state as

$$p_r\simeq\sqrt{8\pi N}\exp(-N)\,r^{2N}\eta^{N/2} \tag{4.22}$$

(see [150] for details). It is obvious that, for small r, $\eta\ll 1$ (a lossy channel); this probability is too small for large N, which limits the practical use of the proposed method.

We briefly summarize the existing problems with obtaining $N00N$ states. The experimental results show the feasibility of obtaining $N00N$ states with the number of photons $N<10$ using quantum optics methods. Obtaining the required meso- ($N\propto 10^2$–10^3) and macroscopic ($N\gg 10^3$) optical $N00N$ states is a nontrivial and still unsolved problem. There are at least two fundamental circumstances that hamper the use of $N00N$ states with a relatively large number of photons N in practice and significantly reduce the visibility of the N-photon interference pattern.

First, as discussed above, the detection of states containing a definite (and large) number of photons is an unresolved technological problem.

Second, a significant problem is the sensitivity of $N00N$ states to photon losses. Indeed, if we take into account that the $N00N$ state is a maximally path-entangled state, whose properties are associated with the uncertainty in the location of photons relative to two spatial modes, the loss of a single photon (which from the standpoint of quantum mechanics is equivalent to making a measurement) leads to the collapse of state (2.44) with an equal probability of 1/2 to Fock states $|N-1,0\rangle$ or $|0,N-1\rangle$, which no longer have any advantages for quantum metrology. In this regard, it makes sense to study the critical values of the number of photons at which the $N00N$ states can still be useful for quantum metrology problems at a reasonable (from an experimental standpoint) loss level.

5. Quantum metrology with particle loss

5.1 Fictitious beamsplitter method

The effect that the loss of photons in an MZI has on the accuracy of measurements can be studied in a sufficiently general form based on the method of fictitious beamsplitters (FBSs) mentioned above, as shown in Fig. 9. The purpose of these elements is to account for the interaction of the interferometer with the environment, which is accompanied by decoherence and the loss of a small number of particles from the interferometer channels. In particular, the FBS method was used to study the applicability of $N00N$ states to practical problems in quantum metrology [153–156]. The various strategies proposed in these studies to achieve the

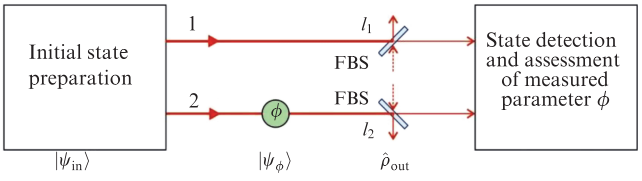

Fig. 9. Effective quantum metrology schematic with particle loss. Interaction with environment in each channel is ensured using fictitious beamsplitters (FBS), which randomly remove l_1 and l_2 particles from corresponding channel. Dotted arrows indicate vacuum noise introduced into measurement system by the environment.

maximum available accuracy of estimating an a priori unknown phase show that the ideal (symmetric) $N00N$ state may not be the optimum one in the presence of losses; entangled Fock states, asymmetric $N00N$ states, and certain two-mode states turn out to be more useful [154, 155, 157]. Importantly, in an optical experiment within dissipative quantum metrology studies, real (not fictitious) beamsplitters can be used for controlled decoherence of the system.

Let us consider the diagram shown in Fig. 9; it reflects the procedure for measuring the phase shift ϕ in the presence of losses. Let a two-mode state as in (4.20) be fed to the entrance to the interferometer (cf. [158]). We then take the phase shift in the interferometer arms into account, assuming the first mode to be a reference one for simplicity. Then, only the second mode gains a phase shift ϕ described by the operator

$$\hat{U}_\phi = \exp\left(\mathrm{i}\phi(\hat{a}_2^\dagger \hat{a}_2)^k\right) \tag{5.1}$$

which gives rise to the state $|\psi_{\text{out}}\rangle = \hat{U}_\phi|\psi_{\text{in}}\rangle$,

$$|\psi_{\text{out}}\rangle = \sum_{m=0}^{N} A_m \exp\left(\mathrm{i}\phi m^k\right)|N-m,m\rangle\,, \tag{5.2}$$

where, as previously, k is the 'nonlinearity degree' of quantum metrology. It is worth noting that, for $k=1$, operator (5.1) is physically equivalent to the previously used operator (2.28). After two FBSs, state (5.2) becomes (see [155])

$$|\psi_{\text{out}}\rangle = \sum_{l_1=0}^{N}\sum_{l_2=0}^{N-l_1}\sum_{m=l_2}^{N-l_1} A_m\sqrt{B^m_{l_1,l_2}}\,\exp\left(\mathrm{i}\phi m^k\right) \times |N-m-l_1, m-l_2\rangle \otimes |l_1,l_2\rangle\,, \tag{5.3}$$

where $l_{1,2}$ is the number of photons lost in respective channels 1 and 2, and $|l_1,l_2\rangle$ is the Fock state of the lost photons. In (5.3), we introduce the coefficient

$$B^m_{l_1,l_2} = C^{l_1}_{N-m} C^{l_2}_m \eta_1^{N-m}(\eta_1^{-1}-1)^{l_1}\eta_2^m(\eta_2^{-1}-1)^{l_2} \tag{5.4}$$

to characterize the corresponding probability amplitudes of Fock modes in the presence of particle losses [157]. In (5.4), C^k_n are the binomial coefficients and $\eta_{1,2} \leqslant 1$ are the FBS transmittance coefficients in the interferometer arms. Importantly, the phase shift operator (for example, (2.28)) commutes with the FBS operator [11]. This means that the FBS can formally be placed anywhere in the setup in Fig. 9: from the preparation of the initial state to the detection of the final state $|\psi_{\text{out}}\rangle$. It is therefore irrelevant whether the particles were lost before, during, or after the phase shift: the accuracy of the measurement does not change.

Because the lost particles $l_{1,2}$ are not detected, it is convenient to eliminate the states $|l_1,l_2\rangle$ from (5.3). For this, we use the density matrix $|\psi_{\text{out}}\rangle\langle\psi_{\text{out}}|$ and trace it over the $|l_1,l_2\rangle$ state. As a result, we obtain the density matrix of the (spatially) mixed two-mode state of particles that remain in the interferometer and participate in the measurement [155],

$$\hat{\rho}_{\text{out}} = \sum_{l_1=0}^{N}\sum_{l_2=0}^{N-l_1} p_{l_1,l_2}\left|\xi_{l_1,l_2}(\phi)\right\rangle\left\langle\xi_{l_1,l_2}(\phi)\right|, \tag{5.5}$$

where

$$\left|\xi_{l_1,l_2}(\phi)\right\rangle = \frac{1}{\sqrt{p_{l_1,l_2}}}\sum_{m=l_2}^{N-l_1} A_m\sqrt{B^m_{l_1,l_2}}\,\exp\left(\mathrm{i}\phi m^k\right) \times |N-m-l_1, m-l_2\rangle\,, \tag{5.6}$$

with $p_{l_1,l_2} \equiv \sum_{m=l_2}^{N-l_1}|A_m|^2 B^m_{l_1,l_2}$. State (5.5) is a universal tool for describing quantum metrology based on two-mode states with particle losses taken into account. The amplitudes A_m in (5.6) allow unambiguously describing the quantum state of the system both at the initial instant, Eqn (5.2), and after the loss of particles, Eqns (5.5) and (5.6), and calculating the QFI, as we show below.

5.2 Metrology accuracy assessment in the case of particle number dissipation. Optimum states

We estimate the maximum accuracy of quantum metrology in the case of particle dissipation in terms of the QCRB in Eqn (2.8). For simplicity, we restrict ourselves to linear quantum metrology, setting $k=1$ in (5.6). Because we are dealing with mixed states, calculating the QFI requires using expression (2.10); such a calculation is nontrivial in general, but in the case where the density matrix is represented in standard form (5.5), the method proposed in [155] allows estimating the QFI of a mixed state as a weighted sum of QFIs calculated for each term in (5.5) separately:

$$\tilde{F}_q = 4\sum_{l_1=0}^{N}\sum_{l_2=0}^{N-l_1} p_{l_1,l_2}\left(\langle\partial_\phi\xi_{l_1,l_2}|\partial_\phi\xi_{l_1,l_2}\rangle - \left|\langle\partial_\phi\xi_{l_1,l_2}|\xi_{l_1,l_2}\rangle\right|^2\right). \tag{5.7}$$

In all cases, $F_q \leqslant \tilde{F}_q$ due to the convexity and additivity properties of the QFI, Eqns (2.16) and (2.17) (also see [155]). An important point is that, in application to quantum metrology, the difference $F_q - \tilde{F}_q$ is formed due to the nonorthogonality of the vectors $|\xi_{l_1,l_2}(\phi)\rangle$ with a fixed total number of lost particles $l = l_1 + l_2$ (see. (5.6)). In turn, this nonorthogonality is due to the lack of information about exactly how many particles were lost from each arm of the MZI. This problem does not occur if the losses can in principle be observed from only one arm of the interferometer, for example, $\eta_2 < 1 = \eta_1$ when the losses are entirely due to the phase shift and/or detection of the parity of the number of particles in arm 2: we then have $\tilde{F}_q = F_q$. Also, $\tilde{F}_q = F_q$ for the $N00N$ state in (2.44), because the loss of a particle from one of the MZI arms can then be unambiguously identified by the Fock state to which the $N00N$ state reduces. In other cases considered here, $\tilde{F}_q \leqslant F_q$. However, as was also shown in [155], $\tilde{F}_q$ and F_q are very close, and such an approximation is justified. Substituting (5.5) in (5.7), we obtain

$$\tilde{F}_q = 4\left[\sum_{m=0}^{N} m^2 A_m^2 - \sum_{l_2=0}^{N}\sum_{l_1=0}^{N-l_2}\frac{\left(\sum_{m=l_2}^{N-l_1} m A_m^2 B^m_{l_1,l_2}\right)^2}{\sum_{m=l_2}^{N-l_1} A_m^2 B^m_{l_1,l_2}}\right]. \tag{5.8}$$

In the case of particle loss, with interferometer transmittance $\eta < 1$, it is useful to introduce a *classical* bound for the accuracy of quantum metrology with losses, the so-called standard interferometric limit (SIL), which is in fact the *limit of the classical metrology* with losses and with the interferometer transmittance η taken into account [155, 157]. The SIL can be calculated by substituting a two-mode binomial-distribution state in (5.8), such that

$$A_m = \frac{1}{\sqrt{2^N}}\sqrt{C^m_N}\,. \tag{5.9}$$

We then have

$$\Delta\phi_{\text{SIL}} = \frac{\sqrt{\eta_1}+\sqrt{\eta_2}}{2\sqrt{\eta_1\eta_2 N}}\,. \tag{5.10}$$

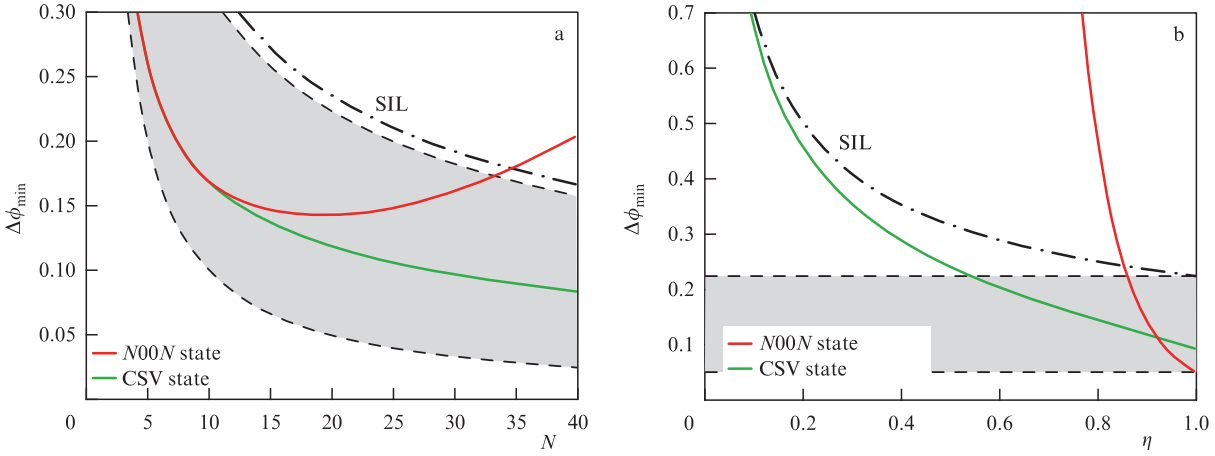

Figure 10. Accuracy of quantum interferometry with particle losses depending (a) on initial average number of photons N for fixed $\eta_1 = \eta_2 = 0.9$ and (b) on MZI transmittance η for a fixed $N = 20$. For squeezed states, $r = 0.88$ is assumed, which gives a good approximation of $\Delta\phi_{\min}$ for $N \gg 1$. Shaded areas indicate fundamental bounds on quantum metrology accuracy within SQL (top) and HL (bottom). SIL is standard interferometric limit in (5.11).

We note that, for a state with distribution (5.9), $F_q = \tilde{F}_q$, and therefore (5.10) is a counterpart of the SQL in the case of particle loss. In the limit of equal losses in the MZI arms, the values of the transmittance coefficients of the MZI arms are equal, $\eta_1 = \eta_2 \equiv \eta$, and (5.10) is simplified to

$$\Delta\phi_{\mathrm{SIL}} = \frac{1}{\sqrt{\eta N}} \tag{5.11}$$

(cf. (2.35)).

The physical meaning of (5.11) is quite simple: ηN is the average number of particles passing through the interferometer and participating in the measurement, while, in the classical limit for the coherent state, $S_{\mathrm{cl}} \equiv F/N = 1$ (see (3.29)).

On the other hand, for the $N00N$ state, we have

$$A_m = \begin{cases} \dfrac{1}{\sqrt{2}}, & m = 0, N, \\ 0, & 0 < m < N, \end{cases} \tag{5.12}$$

and (5.8) gives $F = \tilde{F} = \eta^N N^2$, whence the QCRB in (2.8) becomes (for $\nu = 1$)

$$\Delta\phi_{\mathrm{QCR}} = \frac{1}{N}\sqrt{\frac{\eta_1^N + \eta_2^N}{2\eta_1^N \eta_2^N}}, \tag{5.13}$$

and, in the case of equal transmittance values in the MZI arms,

$$\Delta\phi_{\mathrm{QCR}} = \frac{1}{N\sqrt{\eta^N}}. \tag{5.14}$$

The deterioration of the QFI by η^N times reflects the fragility of $N00N$ states: a measurement is possible only in the case where all the N particles pass through the FBS, and η^N is the probability of such an event. Expression (5.14) allows calculating the number of particles corresponding to the maximum quantum metrology accuracy with $N00N$ states at a given loss level η (Fig. 10). Calculating the derivative of the QFI $F_q = N^2\eta^N$ with respect to N, we find this number of particles N_{c} as

$$N_{\mathrm{c}} = -\frac{2}{\ln(\eta)}. \tag{5.15}$$

In [157], the problem of optimizing input states to maximize the accuracy of quantum metrology was solved numerically with particle losses taken into account. Expression (5.8) was in fact maximized by varying A_m at different η. The $N00N$ states were shown to be optimal for MZI transmittance values $\eta > \eta_{\mathrm{c}} \simeq \exp(-1/N)$. Thus, for the experimentally attainable value $N = 20$, we have $\eta_{\mathrm{c}} \simeq 0.95$, which means that the required loss level $\gamma_{\mathrm{c}} = 1 - \eta_{\mathrm{c}}$ must not exceed 10% for the $N00N$-state quantum metrology to remain applicable in experiment.

Figure 10 shows the metrology accuracy $\Delta\phi_{\min}$ with various nonclassical states for equal values of the transmittance coefficients of the MZI arms $\eta_1 = \eta_2 \equiv \eta$. The quantum metrology limit corresponds to the curves located in the shaded areas determined by the lossless SQL and HL. The red curve shows the quantity $\Delta\phi_{\min}$ obtained with $N00N$ states (5.14); green curves correspond to quantum metrology schemes with the CSV states discussed in Section 2, in the limit $|\alpha|^2 \gg \sinh^2(r)$, with (cf. (3.10) and [14])

$$\Delta\phi \geqslant \sqrt{\frac{\eta\exp(-2r) + 1 - \eta}{\eta N}}, \tag{5.16}$$

where $N \approx |\alpha|^2$. In Figure 10, the squeezing coefficient $r = 0.88$ is small, and hence $\sinh^2(r) \approx 1$, and the above limit is applicable in the range $N \geqslant 9$, for which the green curve in Fig. 10a is constructed.

It follows from Fig. 10a that, already at $N \geqslant 15$ for fixed values of the MZI transmittance η, CSV states provide better accuracy $\Delta\phi_{\min}$ compared with $N00N$ states. On the other hand, as follows from Fig. 10b, at small (overall) losses of photons in the setup (i.e., at $\eta \geqslant \eta_{\mathrm{c}} \simeq 0.95$), the probe $N00N$ states are more optimal in quantum metrology than the CSV states.

6. Quantum photometry, radiometry, and sensing

6.1 Absolute calibration of photodetectors

Photometry, as part of quantum metrology, is currently one of the most interesting areas where the corpuscular properties of light radiation are harnessed to serve practical purposes.

For incoherent light, the total energy of a photon and the photon energy per mode are key photometry characteristics as regards the units of energy and spectral brightness. From the standpoint of measuring the limit characteristics of light radiation associated with fundamental constants (Planck's and Boltzmann's constants, etc.), it makes sense to consider measurements that are independent of the initial number of photons and are only determined by fundamental constraints imposed by vacuum fluctuations of the light field. Back in the 1970s, attention was drawn to the fact that the process of parametric down conversion is quite suitable for these purposes, which allows obtaining noise photons per mode for the signal and idler fields at the output of a quadratically nonlinear crystal [56]. At that time, many interesting and important applications of SPDC were proposed in photometry in dealing with the generation of states with a definite number of photons and so on. The main 'drawback' of the first experiments, which corroborated these ideas, was the low efficiency of single-photon detectors,[3] which essentially made the proposed photometric methods and approaches ineffective in practice. However, at present, in view of the progress in the design and production of new highly efficient photon detectors, there is a tendency to return to early proposals of quantum photometry, but at the current stage of development of quantum optical technologies in the world. In this review, we only outline the fundamental and practically important avenues in modern quantum metrology and sensing.

We consider the propagation of photons of a signal (s) and an idler (i) field in a medium with quadratic susceptibility. For brevity, we consider the average number of photons per mode at the exit from the medium; in the Heisenberg representation and in the two-mode approximation, it can be represented as (cf. [159])

$$\langle \hat{n}_{\rm s}(t)\rangle = \langle \hat{n}_{\rm s}(0)\rangle \cosh^2(\Gamma t) + \langle \hat{n}_{\rm i}(0)\rangle \sinh^2(\Gamma t) + \sinh^2(\Gamma t)\,, \tag{6.1}$$

$$\langle \hat{n}_{\rm i}(t)\rangle = \langle \hat{n}_{\rm i}(0)\rangle \cosh^2(\Gamma t) + \langle \hat{n}_{\rm s}(0)\rangle \sinh^2(\Gamma t) + \sinh^2(\Gamma t)\,, \tag{6.2}$$

where $\langle \hat{n}_{\rm s,i}(0)\rangle$ is the average number of signal and idler field photons at the input to the crystal (at the instant $t = 0$) and Γ is the gain increment, proportional to the amplitude of classical pumping of the crystal and its effective quadratic susceptibility. In (6.1) and (6.2), the 'cross' correlators of the creation/annihilation operators of photons belonging to different modes are omitted, because we are interested in only the vacuum and/or thermal states of light radiation at the entrance to the medium. The last term in (6.1) and (6.2) is independent of the initial number of photons and is due to the contribution of vacuum fluctuations. They play a key role in various measuring devices that use the quantum properties of SPDC radiation, with $\langle \hat{n}_{\rm s,i}(0)\rangle = 0$ in (6.1), (6.2).

Because each biphoton production event in SPDC occurs at one space–time 'point,' biphotons can be used for absolute calibration of detectors. Figure 11 shows a diagram of the absolute calibration of detectors based on SPDC. The idea of this method is quite simple. We assume that, over some observation time $t = \tau_{\rm obs}$, SPDC produces N biphoton pairs on average. Two independent detectors with unknown quantum efficiencies $\eta_{\rm s,i}$ then measure the average number of photons $\langle \hat{n}_{\rm s,i}\rangle$ in each field, and hence

$$\langle \hat{n}_{\rm s}(\tau_{\rm obs})\rangle = \eta_{\rm s} N\,, \qquad \langle \hat{n}_{\rm i}(\tau_{\rm obs})\rangle = \eta_{\rm i} N\,. \tag{6.3}$$

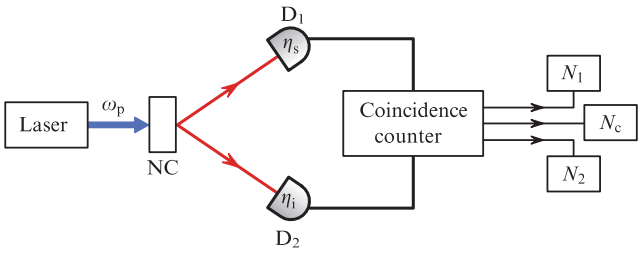

Figure 11. Schematic of absolute calibration of single-photon detectors based on SPDC. $\eta_{\rm s,i}$ is the detector efficiency, NC is a nonlinear crystal, $N_{1,2}$ are the numbers of activations of detectors 1 and 2, and $N_{\rm c}$ is the number of joint activations.

In addition, the number of coincidences $\langle \hat{n}_{\rm c}\rangle$ measured at the exit from the crystal during the same time period is given by

$$\langle \hat{n}_{\rm c}(\tau_{\rm obs})\rangle = \eta_{\rm s}\eta_{\rm i} N\,. \tag{6.4}$$

It follows from (6.3) and (6.4) that the detector efficiencies are

$$\eta_{\rm s} = \frac{\langle \hat{n}_{\rm c}(\tau_{\rm obs})\rangle}{\langle \hat{n}_{\rm s}(\tau_{\rm obs})\rangle}\,, \qquad \eta_{\rm i} = \frac{\langle \hat{n}_{\rm c}(\tau_{\rm obs})\rangle}{\langle \hat{n}_{\rm i}(\tau_{\rm obs})\rangle} \tag{6.5}$$

and are independent of N. Importantly, expressions (6.5), strictly speaking, determine not the efficiency of the detectors themselves but the measurement efficiency of the entire setup in Fig. 11, including possible losses on optical elements.

In [118], a comparative analysis is given of methods for calibrating detectors, including the traditional method based on measuring the radiation power (substitution method) and the methods based on detector calibration with correlated photon pairs considered here. The destructive processes affecting the measurement error are discussed. Overall, the total relative measurement uncertainty for the substitution method and the correlated photon pair method is respectively 0.17% and 0.18%. The advantage of the latter method is that the parameters of one of the detectors (for example, in the idler wave channel) can be known a priori (for example, from other measurements), and then the properties of the unknown detector in the other signal wave channel are to be determined. In this case, it is possible to calibrate both semiconducting avalanche diodes that do not distinguish the number of photons and the TES (transition-edge sensor) detectors, which resolve the number of photons. Relatively recently, the method of correlated photon pairs was adapted for the calibration of TES detectors with a relative uncertainty of 10^{-3} [160].

Significant effort is devoted to reference-free calibration, not of counting photodetectors, but of analogue ones, including in the terahertz frequency range. When using analogue detectors, a current is recorded that is a superposition of many photopulses or detector responses to the external light field [161],

$$i(t) = \sum_{k=1}^{m} q_k f(t - t_k)\,, \tag{6.6}$$

[3] In the 1970s–1990s, the main instrument to detect ultra-weak light fields was photomultiplier tubes, whose quantum efficiency was about 10 to 15%.

where q_k is the charge carried by a single-photon response pulse and f is a function describing its temporal form. In such experiments, parametric down conversion is typically used in the high-gain (so-called twin-beam) regime. Convenient nonclassicality measures are the covariance $C = \langle \delta i_s \delta i_i \rangle / (\langle i_s \rangle + \langle i_i \rangle)$ and/or the difference photocurrent noise reduction factor (NRF), which is proportional to the two-mode squeezing factor. These measures are calculated from current measurements at the exit from optical detectors in the signal (s) and idle (i) channels.

For example, in [162, 163], the NRF and the relative covariance of currents measured in the signal and idle channels with conventional analogue photodetectors were considered. General expressions were obtained that allow developing approaches to reference-free measurement of the quantum efficiency of sensitive elements for a wide class of conventional analogue detectors. It turns out that, in order to determine their quantum efficiency, in addition to direct measurements of the current NRF, several approximation procedures have to be used to predetermine the parameters of single-photon responses of the detectors, the average charge $\langle q_k \rangle$ and the dispersion Δq_k. The quantum efficiency of analogue detectors can possibly be determined much more conveniently and more accurately from the covariance of the signal and idle currents [164].

We note that, although the reference-free calibration method has been widely tested on counting and analogue detectors, there have been no studies yet where it would be scaled to detectors with photon number resolution, whose detection efficiency depends on the number of photons itself [118]. Moreover, measuring an arbitrary observable in quantum theory is an independent and often nontrivial problem. In this regard, of particular importance are the procedures for measuring a certain set of POVM operators $\{\hat{\Pi}_k\}$ that characterize an initial quantum state described by the density operator $\hat{\rho}$: upon detection, a certain k is obtained with the probability

$$p_k = \mathrm{tr}\,[\hat{\Pi}_k \hat{\rho}]\,, \tag{6.7}$$

where $\hat{\Pi}_k \geqslant 0$ and $\sum \hat{\Pi}_k = 1$.

Currently, to calibrate photon-resolving detectors that allow the detection of a definite number of photons, a quantum tomography procedure has been demonstrated for detectors with probe coherent radiation whose density operator is $\hat{\rho} = |\alpha_j\rangle\langle\alpha_j|$. In this case, (6.7) can be written as a matrix equation, and hence

$$p_{j,k} = \sum_{n=0}^{M} F_{j,n}\, \Pi_{n,k}\,, \tag{6.8}$$

where $F_{j,n} \equiv \exp(-|\alpha_j|^2)|\alpha_j|^{2n}/n!$, $\Pi_{n,k}$ are diagonal elements of the operator $\hat{\Pi}_k = \sum_{n=0}^{M} \Pi_{n,k} |n\rangle\langle n|$, taken in the Fock state basis, and M is the maximum number of photons that a given detector can resolve. Inverting (6.7) allows reconstructing the unknown elements $\Pi_{n,k}$ given the results for the measured probabilities $p_{j,k}$ and the known probe (coherent) states, the elements $F_{j,n}$. Moreover, their number depends on whether we use the coherent field phase α_j (phase-sensitive tomography) or the phase-insensitive tomography procedure. In the first case, the matrix $\Pi_{n,k}$ contains $N \times M^2$ elements, and, in the second, $N \times M$ elements. In [165], the authors could reconstruct the $\Pi_{n,k}$ for a detector that resolves up to eight photons. It turned out that the tomography procedure is quite resistant to fluctuations in the energy of the initial state pulses. Using a mixture of coherent Gauss-distributed probe states with a distribution width of $0.02|\alpha_j|^2$ instead of pure states ultimately led to a relative error of only 0.7% in determining $\Pi_{n,k}$.

In our view, the quantum tomography method is relevant when the number of photons M resolved by a detector is relatively small. As M increases, the tomography procedure requires many measurements and, in the future, in creating detectors that would resolve a large number of photons, will become a time-consuming and rather cumbersome problem. An urgent task, obviously, is therefore to optimize such a procedure based on methods and approaches of quantum machine learning, which are already used in the tomography of quantum states of a light field [166].

6.2 Vacuum fluctuations as a metrology reference for light brightness

Recently, the measurement and quantum assessment of temperature as a (fluctuating) parameter of physical systems of various natures has been gaining increasing interest (see, e.g., [167, 168]).

In particular, it is shown in [167] that SQL measurements (estimates) of the inverse temperature parameter $\beta = (k_B T)^{-1}$ for a 'thermometer' made of N test particles (modes) can be specified in the form

$$\Delta\beta \geqslant \frac{1}{\sqrt{N}\sqrt{|\mathrm{d}\bar{\epsilon}/\mathrm{d}\beta|}}\,, \tag{6.9}$$

where $\bar{\epsilon}$ is the average internal energy per particle (mode). Improved temperature measurements are also possible using $N00N$ probe states (cf. [136]).

In the context of the optical quantum metrology methods discussed in this review, it is worth noting that the TES photon detectors mentioned above are in fact the same sensors that distinguish the energy of photons, but operate in the range of low temperatures (100 mK and below) [169]. Their efficiency is already approaching 100%: for example, the efficiency of titanium-based TESs is 98% at a wavelength of 850 nm [170].

In the range of high temperatures (room and above), the development of quantum sensors is still gaining momentum. In this regard, it is interesting to note study [171], where the authors achieved an accuracy of 80 nK $\mathrm{Hz}^{-1/2}$ in measuring temperature using the thermo–optical effect of whispering gallery modes for a CaF_2 microcavity; the additional phase shift for the selected modes is due to a change in the refractive index due to heating of the material. It would be interesting to develop this measurement technique by combining it with the HOM interferometer, which allows using $N00N$ states for precision temperature assessment, as was done in [136] (see also Fig. 12).

Here, we focus on the process of parametric down conversion in quantum metrology and sensing, which is simpler in our opinion and which allows estimating a sufficiently high brightness temperature (exceeding room temperature severalfold) at the level of vacuum fluctuations of light. In view of the advent of photon-resolving detectors, such systems are of interest not only from a fundamental but also from a practical standpoint.

Figure 12 shows the setup of a photometer for measuring the brightness temperature of an unknown incoherent light field source [57, 172, 173]. The measurement proceeds in two

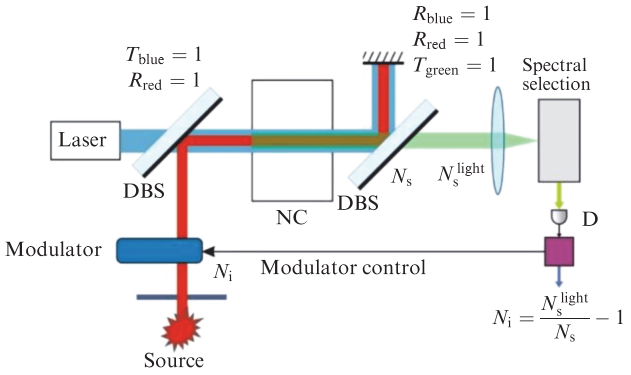

Figure 12. Photometer schematic for measuring brightness temperature of an unknown thermal radiation source with N_i photons per mode. Laser, signal, and idle radiation are respectively shown blue, green, and red. T and R are transmittance and reflection coefficients of the two mirrors (before and after crystal) at corresponding wavelengths, DBS is a dichroic beamsplitter, NC is a nonlinear crystal, and $N_{i,s}$ are average numbers of idler and signal photons detected.

stages. The goal is to measure the number of signal photons $\langle\hat{n}_s(t)\rangle$ per mode over some observation time $t = \tau_{obs}$. At the first stage, the measurement is carried out in the SPDC regime, when the number of photons $\langle\hat{n}_s(\tau_{obs})\rangle$ is measured (per mode) with $\langle\hat{n}_s(0)\rangle = 0$ and $\langle\hat{n}_i(0)\rangle = 0$. At the second stage, the average number of photons $\langle\hat{n}'_s(\tau_{obs})\rangle$ is measured in the signal field when the idler wave port at the crystal input is illuminated by the thermal radiation from an unknown source with the average number of photons

$$\langle\hat{n}_i(0)\rangle = \frac{1}{\exp\left(\hbar\omega_i/(k_B T)\right) - 1}\,, \tag{6.10}$$

where T is the radiation temperature. Thus, the initial average number of photons $\langle\hat{n}_i(0)\rangle$ in the idler wave can be determined from the ratio of the measurement results

$$\frac{\langle\hat{n}'_s(\tau_{obs})\rangle}{\langle\hat{n}_s(\tau_{obs})\rangle} = \langle\hat{n}_i(0)\rangle + 1 = \frac{\exp\left(\hbar\omega_i/(k_B T)\right)}{\exp\left(\hbar\omega_i/(k_B T)\right) - 1}\,, \tag{6.11}$$

where (6.10) is used on the right-hand side.

Expressions (6.9) and (6.10) allow estimating the temperature T of radiation from an unknown thermal source (see Fig. 12). An important property of using this method is the limit in which the idler wave contains only one (thermal) photon per mode on average, i.e., $\langle\hat{n}_i(0)\rangle \simeq 1$. In this case, we are talking about temperature measurements at the level of vacuum fluctuations, which for the idle field wavelength of 1 μm is $T \simeq 2.1 \times 10^4$ K. This allows the photometer to be used as a temperature sensor for radiation sources with high brightness characteristics. However, when implementing this method for metrological purposes, the above-mentioned difficulties arise, related to the correct accounting for the population of the 'illuminated' modes. In addition, the method requires a careful independent measurement of reflection losses of all elements of the calibrated path.

In the diagram shown in Fig. 12, the number of photons N_i is measured, which is proportional to the spectral brightness of the source. The signal-mode photon numbers

$$N_s = F_s(0 + 1) = F_s\,, \tag{6.12}$$

$$N_s^{light} = F_s(N_i + 1) \tag{6.13}$$

are respectively measured at the closed and open positions of the intensity modulator, and

$$F_s = 4\pi^2\omega_s\omega_i c^{-2}\chi^{(2)}(\omega_s = \omega_p - \omega_i)|E_p|^2 l^2 \tag{6.14}$$

is the so-called parametric conversion coefficient (with $\chi^{(2)}$ being the quadratic susceptibility of the crystal, E_p the laser pump field amplitude, and l the crystal length).

An interesting spin-off of this method, which requires further development today, is the use of a multimode N regime, which, even in the case of independent modes, can give a gain of $\sqrt{N}$, corresponding to the SQL. A more important case is where entangled states of these modes are used, which would allow overcoming SQL measurements and temperature estimates, reaching genuinely quantum bounds for its measurement. The method for measuring spectral brightness was adapted to the terahertz range in [174].

7. Conclusions

We have discussed the current level of modern optical quantum metrology and its possible impact on the development of other areas that are currently associated with quantum technologies. We presented relevant theoretical approaches to quantum assessment of unknown parameters in optics and discussed experimental methods for their measurement based on a POVM of observable quantities and photon number parity measurements, which allow achieving a minimum error in measuring and assessing an a priori unknown phase parameter. Particular attention is paid to the generation and use of nonclassical (squeezed, maximally entangled in space, macroscopically superpositional, and so on) states of light radiation in such measurements; the main facts about their QFI are summarized in Table 1. To achieve a maximum accuracy of measurements of unknown phase parameters (maximum in terms of the number of photons), we discussed both linear quantum metrology setups and nonlinear ones, where the unknown phase parameter depends on the number of photons.

As regards the practical aspect, we have discussed various quantum metrology schemes: Mach–Zehnder, Michelson, and Hong–Ou–Mandel interferometers and their combinations, which are currently used to measure the characteristic length difference, temperature variations, concentrations of substances, and so on at the level of quantum limitations. Particular attention is paid to the analysis of measurement accuracy in the case of photon losses, imperfections of the optical element base, detectors, etc. A considerable part of the review is devoted to the new possibilities of quantum metrology that have recently opened up due to the use of various photon-resolving detectors.

Although the content of this review is quite vast, many important areas of quantum metrology and sensing have not been discussed. First and foremost are quantum measurements and metrology carried out with atomic media. In the Introduction, we only outlined the corresponding areas — optical clocks, gyroscopes, gravimeters, and magnetometers — which are actively being developed in the world today and which can be useful in navigation, environmental monitoring, searching for minerals, etc.

We did not discuss the problem of quantum metrology with two or more (a priori unknown) phase parameters. This problem is of great practical interest and has potential in view of the creation of spatially distributed networks of quantum

sensors (see, e.g., [175]). As theoretical analysis shows, the multimode $N00N$ state no longer saturates the QFI in this case [176]. In addition, for the same reasons, the strategies for optimal quantum estimation and measurement seem to be more diverse here [177], requiring multiparameter squeezing or entanglement (see, e.g., [178]). Analyzing multiparameter quantum metrology and sensing requires a separate discussion, including particular application areas that are still in their infancy. Obviously, this review, which covers modern theoretical and experimental methods and approaches in quantum metrology together with the state of the art of quantum technologies in general, can be a starting point for this kind of research in the future.

The study was supported by the Ministry of Science and Higher Education of the Russian Federation at the Federal State Autonomous Educational Institution of Higher Education, South Ural State University (agreement 075-15-2022-1116 dated 07/01/2022). S P K is grateful to the Interdisciplinary Scientific and Educational School of Moscow University Photonic and Quantum Technologies: Digital Medicine for support.

References

1. Imkamp D, Schmitt R, Berthold J *Tech. Messen* **79** (10) 433 (2012) https://doi.org/10.1524/teme.2012.0251
2. Imkamp D et al. *J. Sens. Sens. Syst.* **5** 325 (2016) https://doi.org/10.5194/jsss-5-325-2016
3. Pendrill L R, NCSLI Measure, https://www.euramet.org/
4. Catalucci S et al. *Int. J. Adv. Manuf. Technol.* **120** 4271 (2022)
5. Born M, Wolf E *Principles of Optics* (Oxford: Pergamon Press, 1968); Translated into Russian: *Osnovy Optiki* (Moscow: Nauka, 1973)
6. Caves C M *Phys. Rev. D* **23** 1693 (1981)
7. Unruh W G, in *Quantum Optics, Experimental Gravity, and Measurement Theory* (Eds P Meystre, M O Scully) (New York: Plenum Press, 1983) p. 647
8. Nawrocki W *Introduction to Quantum Metrology*: *Quantum Standards and Instrumentation* (Cham: Springer, 2015)
9. Lawall J, Kessler E *Rev. Sci. Instrum.* **71** 2669 (2000)
10. Braginskii V B *Sov. Phys. JETP* **26** 831 (1968); *Zh. Eksp. Teor. Fiz.* **53** 1434 (1967)
11. Demkowicz-Dobrzański R, Jarzyna M, Kolodyński J *Prog. Opt.* **60** 345 (2015)
12. Dodonov V V, Man'ko V I *Invariants and the Evolution of Nonstationary Quantum Systems* (Proc. of the Lebedev Physics Institute, Vol. 183) (Commack, NY: Nova Science, 1989); Translated from Russian: in *Invarianty i Evolyutsiya Nestatsionarnykh Kvantovykh Sistem* (Trudy Fiz. Inst. Akad. Nauk SSSR, Vol. 183) (Moscow: Nauka, 1987)
13. Thompson J D et al. *Nature* **452** 72 (2008)
14. Schnabel R *Phys. Rep.* **684** 1 (2017)
15. Zurek W H, in *Complexity, Entropy and The Physics of Information* (Ed. W H Zurek) (Santa Fe: SFI Press, 2023) p. 437
16. Unruh W G *Ann. New York Acad. Sci.* **480** 242 (1986) https://doi.org/10.1111/j.1749-6632.1986.tb12427.x
17. Danilishin S L, Khalili F Ya, Miao H *Living Rev. Relativ.* **22** 2 (2019) https://doi.org/10.1007/s41114-019-0018-y
18. Aasi J et al. *Nature Photon.* **7** 613 (2013) https://doi.org/10.1038/nphoton.2013.17
19. Braginsky V B *Fizicheskie Eksperimenty s Probnymi Telami* (Physical Experiments with Test Bodies) (Moscow: Nauka, 1970)
20. Press W H, Thorne K S "Gravitational-wave astronomy", Preprint (Pasadena, CA: California Institute of Technology, 1972); Translated into Russian: *Usp. Fiz. Nauk* **110** 569 (1973)
21. Abbott B P et al. (KAGRA Collab., LIGO Scientific Collab., Virgo Collab.) *Living Rev. Relativ.* **23** 3 (2020) https://doi.org/10.1007/s41114-020-00026-9
22. Scully M O, Zubairy M S *Quantum Optics* (Cambridge: Cambridge Univ. Press, 1997); Translated into Russian: *Kvantovaya Optika* (Moscow: Fizmatlit, 2003)
23. Khalili F Ya *Phys. Usp.* **59** 968 (2016); *Usp. Fiz. Nauk* **186** 1059 (2016)
24. Ludlow A D et al. *Rev. Mod. Phys.* **87** 637 (2015)
25. Mitchell M W, Palacios Alvarez S *Rev. Mod. Phys.* **92** 021001 (2020)
26. Ono T, Okamoto R, Takeuchi S *Nat. Commun.* **4** 2426 (2013) https://doi.org/10.1038/ncomms3426
27. Acín A et al. *New J. Phys.* **20** 080201 (2018)
28. Bongs K et al. *Nat. Rev. Phys.* **1** 731 (2019)
29. Pezzè L et al. *Rev. Mod. Phys.* **90** 035005 (2018)
30. Degen C L, Reinhard F, Cappellaro P *Rev. Mod. Phys.* **89** 035002 (2017)
31. Migdall A et al. (Eds) *Single-Photon Generation and Detection*: *Physics and Applications* (Experimental Methods in the Physical Sciences, Vol. 45) (Boston: Academic Press, 2013)
32. Bloch I *Nature Phys.* **1** 23 (2005)
33. Marti G E et al. *Phys. Rev. Lett.* **120** 103201 (2018)
34. Gross C et al. *Nature* **464** 1165 (2010)
35. Wolfgramm F et al. *Phys. Rev. Lett.* **105** 053601 (2010)
36. Leroux I D, Schleier-Smith M H, Vuletić V *Phys. Rev. Lett.* **104** 250801 (2010)
37. Jackson Kimball D F et al. "Optical magnetometry with modulated light", in *Optical Magnetometry* (Eds D Budker, D F Jackson Kimball) (Cambridge: Cambridge Univ. Press, 2013) p. 104, https://doi.org/10.1017/CBO9780511846380.007
38. Wasilewski W et al. *Phys. Rev. Lett.* **104** 133601 (2010)
39. Lee S K et al. *Appl. Phys. Lett.* **89** 214106 (2006)
40. Afanasiev A E et al. *Opt. Laser Technol.* **148** 107698 (2022)
41. Sewell R J et al. *J. Phys. B* **43** 051003 (2010)
42. Degen C L, Reinhard F, Cappellaro P *Rev. Mod. Phys.* **89** 035002 (2017)
43. Kulik S P *Nauka Innov.* (8) 31 (2023)
44. Tsarev D V et al. *New J. Phys.* **21** 083041 (2019)
45. Starodumov A N et al. *Appl. Phys. Lett.* **70** 19 (1997)
46. Boto A N et al. *Phys. Rev. Lett.* **85** 2733 (2000)
47. Kok P, Braunstein S L, Dowling J P *J. Opt. B* **6** S811 (2004)
48. Ball P *Physics* **8** 18 (2015) https://doi.org/10.1103/Physics.8.18
49. Dowling J P, Seshadreesan K P *J. Lightwave Technol.* **33** 2359 (2015)
50. Cohen L et al. *Phys. Rev. Lett.* **123** 203601 (2019)
51. Shapiro J H *IEEE Aerospace Electron. Syst. Mag.* **35** 8 (2020)
52. Pezzé L, Smerzi A *Phys. Rev. Lett.* **100** 073601 (2008)
53. Lang M D, Caves C M *Phys. Rev. Lett.* **111** 173601 (2013)
54. Manceau M, Khalili F, Chekhova M *New J. Phys.* **19** 013014 (2017)
55. Tichy M C *J. Phys. B* **47** 103001 (2014)
56. Klyshko D N *Sov. J. Quantum Electron.* **7** 591 (1977); *Kvantovaya Elektron.* **4** 1056 (1977)
57. Klyshko D N, Penin A N *Sov. Phys. Usp.* **30** 716 (1987); *Usp. Fiz. Nauk* **152** 653 (1987)
58. Zwinkels J C et al. *Metrologia* **47** R15 (2010)
59. Chu Y et al. *Appl. Phys. Lett.* **118** 240401 (2021)
60. Polino E et al. *AVS Quantum Sci.* **2** 024703 (2020)
61. Dowling J P *Contemp. Phys.* **49** 125 (2008)
62. Baburin A S et al., in *2022 Intern. Conf. Laser Optics, ICLO, Saint Petersburg, Russian Federation, 20–24 June 2022* (Piscataway, NJ: IEEE, 2022) https://doi.org/10.1109/ICLO54117.2022.9839948
63. Chekhova M V, Ou Z Y *Adv. Opt. Photon.* **8** 104 (2016)
64. Helstrom C W *Quantum Detection and Estimation Theory* (New York: Academic Press, 1976); Translated into Russian: *Kvantovaya Teoriya Proverki Gipotez i Otsenivaniya* (Moscow: Mir, 1979)
65. Akhmanov S A, D'yakov Yu E, Chirkin A S *Vvedenie v Statisticheskuyu Radiofiziku i Optiku* (Introduction to Statistical Radiophysics and Optics) (Moscow: Nauka, 1981)
66. Giovannetti V, Lloyd S, Maccone L *Phys. Rev. Lett.* **96** 010401 (2006)
67. Bachor H-A, Ralph T C *A Guide to Experiments in Quantum Optics* (Weinheim: Wiley-VCH, 2004) https://doi.org/10.1002/9783527619238
68. Murzakhmetov B K, Chizhov A V *Phys. Part. Nucl.* **27** 309 (1996); *Fiz. Elem. Chastits At. Yadra* **27** 747 (1996)
69. Alodjants A P, Arakelian S M *J. Mod. Opt.* **46** 475 (1999)
70. Yurke B, McCall S L, Klauder J R *Phys. Rev. A* **33** 4033 (1986)
71. Zare R N *Angular Momentum*: *Understanding Spatial Aspects in Chemistry and Physics* (New York: Wiley, 1988); Translated into

Russian: *Teoriya Uglovogo Momenta*: *O Prostranstvennykh Effektakh v Fizike i Khimii* (Moscow: Mir, 1993)
72. Gerry C C, Benmoussa A, Campos R A *J. Mod. Opt.* **54** 2177 (2007)
73. Klyshko D N *J. Exp. Theor. Phys.* **84** 1065 (1997); *Zh. Eksp. Teor. Fiz.* **111** 1955 (1997)
74. Podoshvedov M S, Podoshvedov S A, Kulik S P *Sci. Rep.* **13** 3965 (2023)
75. Podoshvedov M S, Podoshvedov S A *Laser Phys. Lett.* **20** 045202 (2023)
76. Costanzo L S et al. *Phys. Rev. Lett.* **119** 013601 (2017)
77. Pezzé L, Smerzi A *Phys. Rev. Lett.* **110** 163604 (2013)
78. Karasev V P, Masalov A V *Opt. Spectrosc.* **74** 551 (1993); *Opt. Spektrosk.* **74** 928 (1993)
79. Luis A *Phys. Lett. A* **329** 8 (2004)
80. Luis A *Phys. Rev. A* **76** 035801 (2007)
81. Tsarev D V et al. *Opt. Express* **26** 19583 (2018)
82. Zhang J et al. *Opt. Express* **15** 7682 (2007)
83. Sich M et al. *Nature Photon.* **6** 50 (2012)
84. Deng H, Haug H, Yamamoto Y *Rev. Mod. Phys.* **82** 1489 (2010)
85. Khaykovich L et al. *Science* **296** 1290 (2002)
86. Hall M J W, Wiseman H M *Phys. Rev. X* **2** 041006 (2012)
87. Zakharov R V, Tikhonova O V *Phys. Usp.* **66** 381 (2023); *Usp. Fiz. Nauk* **193** 406 (2023)
88. Walls D F *Nature* **306** 141 (1983)
89. Golubev Yu M, Sokolov I V *Sov. Phys. JETP* **60** 234 (1984); *Zh. Eksp. Teor. Fiz.* **87** 408 (1984)
90. Smirnov D F, Troshin A S *Sov. Phys. Usp.* **30** 851 (1987); *Usp. Fiz. Nauk* **153** 233 (1987)
91. Loudon R, Knight P L *J. Mod. Opt.* **34** 709 (1987)
92. Akhmanov S A et al. *Novye Fizicheskie Printsipy Opticheskoi Obrabotki Informatsii* (New Physical Principles of Optical Information Processing) (Eds S A Akhmanov, M A Vorontsov) (Moscow: Nauka, 1990)
93. Kilin S Ya *Kvantovaya Optika*: *Polya i Ikh Detektirovanie* (Quantum Optics: Fields and Their Detection) (Minsk: Navuka i Tekhnika, 1990)
94. Teich M C, Saleh B E A *Quantum Opt.* **1** 153 (1989); Translated into Russian: *Usp. Fiz. Nauk* **161** (4) 101 (1991)
95. Klyshko D N, Masalov A V *Phys. Usp.* **38** 1203 (1995); *Usp. Fiz. Nauk* **165** 1249 (1995)
96. Dodonov V V *J. Opt. B* **4** R1 (2002)
97. Mikheev E V et al. *Sci. Rep.* **9** 14301 (2019)
98. Braunstein S L, van Loock P *Rev. Mod. Phys.* **77** 513 (2005)
99. Andersen U L et al. *Nature Phys.* **11** 713 (2015)
100. Takeda S, Furusawa A *APL Photonics* **4** 060902 (2019)
101. Lvovsky A I, in *Photonics*: *Scientific Foundations, Technology and Applications* (Ed. D L Andrews) (New York: John Wiley and Sons, 2015) p. 121, https://doi.org/10.1002/9781119009719.ch5
102. Vahlbruch H et al. *Phys. Rev. Lett.* **117** 110801 (2016)
103. Dutt A et al. *Phys. Rev. Appl.* **3** 044005 (2015)
104. Mondain F et al. *Photon. Res.* **7** (7) A36 (2019)
105. Mehmet M et al. *Opt. Express* **19** 25763 (2011)
106. Grangier P et al. *Phys. Rev. Lett.* **59** 2153 (1987)
107. Demkowicz-Dobrzański R, Banaszek K, Schnabel R *Phys. Rev. A* **88** 041802 (2013)
108. Campos R A, Saleh B E A, Teich M C *Phys. Rev. A* **40** 1371 (1989)
109. Birrittella R J, Alsing P M, Gerry C C *AVS Quantum Sci.* **3** 014701 (2021)
110. Gol'tsman G N et al. *Appl. Phys. Lett.* **79** 705 (2001)
111. Cheng R et al. *Nature Photon.* **17** 112 (2023)
112. Lita A E et al. *J. Lightwave Technol.* **40** 7578 (2022)
113. Cahall C et al. *Optica* **4** 1534 (2017)
114. Sahin D et al. *Appl. Phys. Lett.* **103** 111116 (2013)
115. Marsili F et al. *Nature Photon.* **7** 210 (2013)
116. Hadfield R H *Nature Photon.* **3** 696 (2009)
117. Eaton M et al. *Nature Photon.* **17** 106 (2023)
118. Polyakov S V *Exp. Meth. Phys. Sci.* **45** 257 (2013)
119. Charaev I et al. *Nat. Nanotechnol.* **18** 343 (2023)
120. Mitchell M W, Lundeen J S, Steinberg A M *Nature* **429** 161 (2004)
121. Resch K J et al. *Phys. Rev. Lett.* **98** 223601 (2007)
122. Okamoto R et al. *New J. Phys.* **10** 073033 (2008)
123. Mandel L, Wolf E *Optical Coherence and Quantum Optics* (Cambridge: Cambridge Univ. Press, 1995); Translated into Russian: *Opticheskaya Kogerentnost' i Kvantovaya Optika* (Moscow: Fizmatlit, 2000)
124. Hong C K, Ou Z Y, Mandel L *Phys. Rev. Lett.* **59** 2044 (1987)
125. Burlakov A V et al. *Phys. Rev. A* **64** 041803 (2001)
126. Klyshko D *Physical Foundations of Quantum Electronics* (Eds M Chekhova, S Kulik) (Singapore: World Scientific, 2011); Translated from Russian: *Fizicheskie Osnovy Kvantovoi Elektroniki* (Moscow: Nauka, 1986)
127. Kim H, Kwon O, Moon H S *Sci. Rep.* **11** 20555 (2021)
128. Grice W P, Walmsley I A *Phys. Rev. A* **56** 1627 (1997)
129. Grice W P, U'Ren A B, Walmsley I A *Phys. Rev. A* **64** 063815 (2001)
130. Scott H et al. *Phys. Rev. A* **104** 053704 (2021)
131. Singh S et al., arXiv:2304.13300
132. Klyshko D N *Phys. Usp.* **37** 1097 (1994); *Usp. Fiz. Nauk* **164** 1187 (1994)
133. Yang Y, Xu L, Giovannetti V *Sci. Rep.* **9** 10821 (2019)
134. Crespi A et al. *Appl. Phys. Lett.* **100** 233704 (2012)
135. Barer R, Tkaczyk S *Nature* **173** 821 (1954)
136. Chen Y et al. *npj Quantum Inf.* **5** 43 (2019)
137. Tateda M, Tanaka S, Sugawara Y *Appl. Opt.* **19** 770 (1980)
138. Tsarev D et al. *New J. Phys.* **22** 113016 (2020)
139. Kim H, Park H S, Choi S-K *Opt. Express* **17** 19720 (2009)
140. Melnikov A A et al. *Proc. Natl. Acad. Sci. USA* **115** 1221 (2018)
141. Melnikov A et al. *Adv. Phys. X* **8** 2165452 (2023)
142. Klyshko D N *Sov. Phys. Usp.* **31** 74 (1988); *Usp. Fiz. Nauk* **154** 133 (1988)
143. Pelucchi E et al. *Nat. Rev. Phys.* **4** 194 (2022)
144. Wang J et al. *Nature Photon.* **14** 273 (2020)
145. Matthews J C F et al. *Nature Photon.* **3** 346 (2009)
146. Silverstone J W et al. *Nature Photon.* **8** 104 (2014)
147. van Loock P *Laser Photon. Rev.* **5** 167 (2011)
148. Hofmann H F, Ono T *Phys. Rev. A* **76** 031806 (2007)
149. Israel Y, Rosen S, Silberberg Y *Phys. Rev. Lett.* **112** 103604 (2014)
150. Ulanov A E et al. *Nat. Commun.* **7** 11925 (2016)
151. Afek I, Ambar O, Silberberg Y *Science* **328** 879 (2010)
152. Kok P, Lee H, Dowling J P *Phys. Rev. A* **65** 052104 (2002)
153. Bohmann M, Sperling J, Vogel W *Phys. Rev. A* **91** 042332 (2015)
154. Huver S D, Wildfeuer C F, Dowling J P *Phys. Rev. A* **78** 063828 (2008)
155. Demkowicz-Dobrzanski R et al. *Phys. Rev. A* **80** 013825 (2009)
156. Rubin M A, Kaushik S *Phys. Rev. A* **75** 053805 (2007)
157. Dorner U et al. *Phys. Rev. Lett.* **102** 040403 (2009)
158. Haigh T J, Ferris A J, Olsen M K *Opt. Commun.* **283** 3540 (2010)
159. Shen Y R *The Principles of Nonlinear Optics* (New York: J. Wiley, 1984); Translated into Russian: *Printsipy Nelineinoi Optiki* (Moscow: Nauka, 1989)
160. Avella A et al. *Opt. Express* **19** 23249 (2011)
161. Brida G et al. *J. Opt. Soc. Am. B* **23** 2185 (2006)
162. Prudkovskii P A, Safronenkov D A, Kitaeva G Kh *Opt. Lett.* **47** 4842 (2022)
163. Novikova T I, Leontyev A A, Kitaeva G Kh *JETP Lett.* **116** 353 (2022); *Pis'ma Zh. Eksp. Teor. Fiz.* **116** 343 (2022)
164. Prudkovskii P et al. *Sensors* **21** 4964 (2021)
165. Lundeen J S et al. *Nature Phys.* **5** 27 (2009)
166. Hsieh H Y et al. *Symmetry* **14** 874 (2022)
167. Stace T M *Phys. Rev. A* **82** 011611 (2010)
168. Campbell S et al. *New J. Phys.* **19** 103003 (2017)
169. Rosenberg D et al. *Phys. Rev. A* **71** 061803 (2005)
170. Fukuda D et al. *Opt. Express* **19** 870 (2011)
171. Weng W et al. *Phys. Rev. Lett.* **112** 160801 (2014)
172. Kitaeva G Kh et al. *Sov. Phys. Dokl.* **24** 564 (1979); *Dokl. Akad. Nauk SSSR* **247** 586 (1979)
173. Vlasenko M F, Kitaeva G Kh, Penin A N *Sov. J. Quantum Electron.* **10** 252 (1980); *Kvantovaya Elektron.* **7** 441 (1980)
174. Kitaeva G Kh et al. *Appl. Phys. B* **116** 929 (2014)
175. Ge W et al. *Phys. Rev. Lett.* **121** 043604 (2018)
176. Humphreys P C et al. *Phys. Rev. Lett.* **111** 070403 (2013)
177. Pezzè L *Nature Photon.* **15** 74 (2021)
178. Gessner M, Smerzi A, Pezzè L *Nat. Commun.* **11** 3817 (2020)